

1
2
3
4
5
6
7
8
9
10
11
12
13
14
15
16
17
18
19
20
21
22
23

On the reliability of the AMS ellipsoid by statistical methods

14 S. Guerrero-Suarez*, F. Martín-Hernández

15 *Departamento de Física de la Tierra, Astronomía y Astrofísica I, Universidad Complutense*
16 *de Madrid*
17 *28040 Madrid, Spain*

18 *Instituto de Geociencias (UCM,CSIC), Facultad de Ciencias Físicas.*
19 *28040. Madrid. Spain*

Abstract

24
25
26
27
28
29
30
31
32
33
34
35
36
37
38
39
40
41
42
43
44
45
46
47
48
49
50
51
52
53
54
55

Weak magnetic materials whose susceptibility values are close to the instrument's accuracy show very large errors in the direct evaluation of their ellipsoid parameters. This may lead to misinterpretation of the magnetic fabric, which is often used as geological indicator. In order to estimate the measurement uncertainties, several statistical methods have been proposed. Within the available statistical methods, the Linear Perturbation Analysis (Hext, 1963) and the non-parametric bootstrap (Constable and Tauxe, 1990) technique have been widely used. In this paper, we make a complete study about these methods to estimate their limitations when applied to n measurements of a single sample. We will analyze which method is better in terms of uncertainties, we will determine when the methods do not provide reliable results and we will establish a measuring protocol. For that, we run simulations for the Linear Perturbation Analysis and the non-parametric bootstrap varying i) number of measurements, ii) the instrumental error and iii) the shape parameter and the anisotropy degree of the AMS ellipsoid. The results show that both methods are not reliable when the difference between eigenvalues is too close in relation to the instrumental error, but increasing the number of measurements can improve the results.

46
47
48
49
50
51
52
53
54
55

Keywords: Anisotropy of Magnetic Susceptibility, Bootstrap, Linear Perturbation Analysis, Rock Magnetism

56 *Corresponding author.

57 *Email address:* saguerre@ucm.es (S. Guerrero-Suarez)

1
2
3
4
5
6
7
8
9 **1. Introduction**

10 The Anisotropy of Magnetic Susceptibility (AMS) is the intrinsic property
11 of a material that describes the directional variability of the induced magneti-
12 zation with respect to the applied field. In single crystal specimens, the AMS
13 is related to the crystallographic structure according to Neumann’s law (Bor-
14 radaile, 2003). In polycrystalline specimens, the AMS is determined also by the
15 degree of alignment of their constituent crystallites. The alignment is caused
16 by geological processes in almost all rock types. The water flow in sediments
17 (Hamilton and Rees, 1970), the lava or magmatic flow in volcanic and pluton
18 rocks (Cañón-Tapia et al., 1995; Ernst and Baragar, 1992) or the ductile defor-
19 mation in metamorphic rocks (Hrouda, 1993), are some of the principal processes
20 studied by means of AMS measurements. Because of this, since mid-1970s, the
21 AMS studies have been an important tool in structural geology, petrofabrics
22 and in the interpretation of magnetic fabrics (Rochette et al., 1992; Tarling
23 and Hrouda, 1993; Kodama, 1995; Borradaile and Henry, 1997; Borradaile and
24 Jackson, 2010).

25 The magnetic susceptibility is linear for diamagnetic minerals by definition.
26 For paramagnetic minerals it is also linear for most available magnetic fields.
27 For ferromagnetic minerals, however, there is a weak field range for which the
28 susceptibility can be considered linear and fitted mathematically into a second
29 rank tensor, that is, a 3x3 symmetric matrix \mathbf{K} such that $\mathbf{M} = \mathbf{KH}$ (Dunlop
30 and Özdemir, 2001). Most ferromagnetic minerals show this linear behavior
31 for fields under 0.1 mT (Hrouda, 2002). The typical way to characterize the
32 anisotropy is to calculate the eigenvalues and the orthogonal eigenvectors of the
33 susceptibility tensor and its graphical representation.

34 The usual experimental procedure to calculate the susceptibility matrix consi-
35 stits of measuring bulk susceptibilities along several known directions. Different
36 experimental protocols (sets of directions to measure along) have been proposed;
37 for a revision, see Borradaile (2003) and references therein. The first schemes
38 included six orientations, however, later works increased the number of posi-
39 tions in order to include an estimation of the error in the mathematical fitting
40 of the susceptibility tensor. A 7-orientation scheme and a 13-orientation scheme
41 were proposed by Borradaile and Stupavsky (Borradaile, 2003). Both schemes,
42 7- and 13-orientation, are used in Sapphire Instruments equipment. The KLY
43 series and later MFK devices from AGICO Instruments use however the 15-
44 orientation scheme proposed by Jelinek (1977). More schemes were discussed
45 by Hext (1963) and Jelínek (1978) but did not become popularly used.

46 In order to get a complete AMS analysis from the orientation schemes, it is
47 recommended an estimation of the confidence intervals for the eigenvalues and
48 the confidence ellipses for the eigenvectors. The readings of bulk susceptibility,
49 or data \mathbf{d} , can be expressed as

50
51
52
53
$$\mathbf{d} = \mathbf{Dk} + \mathbf{e} , \tag{1.1}$$

54 where:

- \mathbf{D} is the experimental design-matrix, the matrix of directional cosines of the orientation scheme,
 - \mathbf{k} is the column vector with the six independent elements of the susceptibility tensor
- $$\mathbf{k} = (\mathbf{K}_{11}, \mathbf{K}_{22}, \mathbf{K}_{33}, \mathbf{K}_{12}, \mathbf{K}_{23}, \mathbf{K}_{13})^T \quad (1.2)$$
- \mathbf{e} is a column vector of random errors.

The best-fit for the susceptibility tensor is the result of multiplying the data (\mathbf{d}) by the generalized inverse of matrix \mathbf{D} :

$$\bar{\mathbf{k}} = (\mathbf{D}^T \mathbf{D})^{-1} \mathbf{D}^T \mathbf{d} . \quad (1.3)$$

Two different statistical methods are the most popular to estimate the confidence intervals of the susceptibility tensor: Linear Perturbation Analysis (LPA) (Hext, 1963; Jelínek, 1978), and non-parametric bootstrap (NPB) (Constable and Tauxe, 1990).

In the LPA method, the mean tensor for a number n of specimens (or number n of measurements of one specimen) is calculated by the theory of least squares fitting. To estimate the confidence intervals of the eigenparameters, the errors \mathbf{e} are assumed small, independent and normally distributed. To calculate the confidence ellipses, the eigenvectors distribution is assumed to be a two-dimensional normal distribution with semi-axes aligned along the mean eigenvectors.

Bootstrap analysis has two approaches: parametric and non-parametric bootstrap. The difference lies in the assumptions on the data distribution. The parametric bootstrap assumes a particular data distribution and the non-parametric bootstrap does not (Davison, 1997).

The non-parametric bootstrap analysis is a random re-sampling method with replacement of observations from the original sample. It allows estimating standard errors, bias and confidence intervals for the parameters. In particular, the bootstrap analysis proposed by Constable and Tauxe (1990), a widely method and associated software used in the paleomagnetic community (Tauxe, 2010), is a non-parametric bootstrap. The mean tensor is calculated in the same way than for the LPA method. To calculate the confidence ellipse, the eigenvectors distribution is assumed to be a Kent distribution (also known as Fisher-Bingham 5 distribution).

The problem of the two methods, LPA and NPB, is that both could yield unrealistic results. They strongly depend on the ratio of the instrumental error to the bulk susceptibility, and the ratio of the instrumental error to the differences between eigenvalues. The AMS of a magnetically weak sample, like one of quartz single crystal with $k_{\text{bulk}} \sim 10^{-5}$ [SI] (Tarling and Hrouda, 1993), and an anisotropically weak sample, such as one of calcite with $\lambda_{\text{max}} - \lambda_{\text{min}} \sim 10^{-6}$ [SI] (Schmidt et al., 2006) may not be well-determined. A magnetically weak sample is defined here as a sample whose bulk susceptibility value is close to the instrumental error. An anisotropically weak sample is one for which the differences

1
2
3
4
5
6
7
8
9 between its susceptibility eigenvalues lie within the range of the instrumental
10 error.

11 The instrumental error includes, together with the technical sensitivity, other
12 sources such as thermal drift and/or mechanical drift. These additional sources
13 increase the instrumental error at least one order of magnitude with respect
14 to its technical sensitivity (Biedermann et al., 2013). The sensitivity of the
15 most common commercial instruments is in the range from 10^{-6} [SI] for Sap-
16 phire instruments susceptibility bridge (Borradaile et al., 2008) and Bartington
17 MS2/MS3 (www.bartington.com) to 10^{-8} [SI] for AGICO Instruments (Hrouda
18 and Pokorný, 2011).

19 Both methods (LPA and NPB) have been compared in previous works
20 (Werner, 1997; Owens, 2000b,a; Borradaile, 2003) for the case of multiple spec-
21 imens. The main differences found are the size and orientation of the semiaxes
22 of the confidence ellipses.

23 The goal of this study is to show how the reliability of the LPA and the
24 NPB methods varies according to the instrumental error, the magnitude of the
25 bulk susceptibility and the difference between the eigenvalues. Moreover we will
26 establish validity limits for both methods and a protocol of measure for the case
27 of n measurements of a single specimen.

28 In order to estimate the reliability, we will check if the success rate reaches
29 the confidence level used in the LPA and the NPB methods. The success rate
30 is the probability for the real anisotropy tensor lying inside the estimated confi-
31 dence intervals. We estimate this probability by performing 500 simulations of
32 the calculation of the AMS ellipsoid. We study the reliability for different cases
33 of magnetically and anisotropically weak samples with different instrumental
34 errors and number of measurements.

35 36 37 38 **2. Methodology**

39 We have used a reference tensor, called the real tensor, to check the reliabil-
40 ity. The synthetic data used to run the simulations will be generated from this
41 real tensor and a known error distribution. In each simulation, the LPA and
42 the NPB methods will be used to obtain the AMS eigenparameters and their
43 confidence intervals. For the eigenvectors, the confidence regions are spherical
44 ellipses, whose major and minor semiangles are called η and ζ respectively. We
45 will use the reference tensor to estimate the success rate of both methods.

46 47 48 *2.1. Synthetic data*

49 The synthetic data are represented as a column vector that contains all
50 measurements of the different positions of the chosen scheme. In this work,
51 we have generated synthetic data for a 15-orientation scheme (Jelinek, 1977),
52 typical of AGICO Instruments. In order to create this vector, the following
53 parameters are necessary:

- 54 · \mathbf{K}_{real} : the real tensor, from which we can obtain the three eigenvalues
55 ($\lambda_1, \lambda_2, \lambda_3$) and their eigenvectors ($\mathbf{v}_1, \mathbf{v}_2, \mathbf{v}_3$). The eigenvalues determine

the mean susceptibility defined as $\lambda_{\text{mean}} = (\lambda_1 + \lambda_2 + \lambda_3)/3$, the degree of anisotropy (P) and the shape parameter (U) of the ellipsoid. The anisotropy degree is defined as $P = \lambda_1/\lambda_3$ (Nagata, 1961) and the shape parameter as $U = \frac{2\lambda_2 - \lambda_1 - \lambda_3}{\lambda_1 - \lambda_3}$ (Jelinek, 1981). This two variables (P and U) indicate how the spacing between the eigenvalues is distributed.

- **D**: the design-matrix that contains the directional cosines of the 15-orientation scheme.

- σ : the standard deviation of the instrumental error distribution assuming it follows a normal distribution (Biedermann et al., 2013). Experimentally, the instrumental error cannot be modified, but in this work, σ has been included in the simulations as the percentage of the mean susceptibility λ_{mean} . That is, a σ value of 0.1 would mean an instrumental error of 10% of λ_{mean} . This parameter indicates how magnetically weak the data are.

The real vector that will contain the 15-orientation measures is calculated from the real tensor and the design-matrix as

$$\mathbf{d}_{\text{real}} = \mathbf{D}\mathbf{k}_{\text{real}} , \tag{2.1}$$

where the design matrix is

$$\mathbf{D} = \begin{pmatrix} .5 & .5 & 0 & -1 & 0 & 0 \\ .5 & .5 & 0 & 1 & 0 & 0 \\ 1 & 0 & 0 & 0 & 0 & 0 \\ .5 & .5 & 0 & -1 & 0 & 0 \\ .5 & .5 & 0 & 1 & 0 & 0 \\ 0 & .5 & .5 & 0 & -1 & 0 \\ 0 & .5 & .5 & 0 & 1 & 0 \\ 0 & 1 & 0 & 0 & 0 & 0 \\ 0 & .5 & .5 & 0 & -1 & 0 \\ 0 & .5 & .5 & 0 & 1 & 0 \\ .5 & 0 & .5 & 0 & 0 & -1 \\ .5 & 0 & .5 & 0 & 0 & 1 \\ 0 & 0 & 1 & 0 & 0 & 0 \\ .5 & 0 & .5 & 0 & 0 & -1 \\ .5 & 0 & .5 & 0 & 0 & 1 \end{pmatrix} \tag{2.2}$$

and \mathbf{k}_{real} is the vector with the six independent components of the real susceptibility tensor \mathbf{K}_{real} , as in (1.2).

The known error distribution is used to calculate n simulated measures for each 15 positions (Jelinek, 1977) and to introduce the instrumental error in the real measures (\mathbf{d}_{real}). Then, the synthetic vector used to run the simulations will be calculated from a normal distribution with mean $\mu = d_{\text{real};i}$, where $d_{\text{real};i}$ is the real value for the position i , and standard deviation σ .

1
2
3
4
5
6
7
8
9 *2.2. Linear Perturbation Analysis: Hext method*

10 According to Hext (1963) the mean susceptibility tensor is calculated from
11 (1.3) and the errors \mathbf{e} in (1.1) are assumed random, independent and normally
12 distributed. The confidence intervals for the eigenparameters at the 95% confi-
13 dence level are calculated in the following way:
14

- 15 · For the eigenvalues,

$$16 \lambda_{i,Hext} \pm t_{(1-\alpha/2)}(n^{-1}\sigma\mathbf{a}_{ii}^T(\mathbf{D}^T\mathbf{D})^{-1}\mathbf{a}_{ii})^{1/2},$$

17 where t is the Student's t -distribution for n degrees of freedom, and \mathbf{a}_{ij}
18 is a function of the unit vectors $\mathbf{X}_i, \mathbf{X}_j$ such that $\mathbf{X}_i^T\mathbf{S}\mathbf{X}_j = \mathbf{a}_{ij}\mathbf{s}$ for any
19 symmetric matrix \mathbf{S} for which \mathbf{s} is the six component vector representation
20 (1.2). The estimated variance is
21
22

$$23 \sigma = \sqrt{\frac{\sum \mathbf{e}_i^2}{n_f}},$$

24 where $n_f = N - 6$ is the number of degrees of freedom, in the case of n
25 measures and a design of 15 positions, $N = 15n$. And $\mathbf{e}_i = \mathbf{d}_i - \mathbf{D}_{ij}\bar{\mathbf{k}}_j$ are
26 the residuals.
27

- 28 · For the eigenvectors (\mathbf{v}_i), the confidence regions are ellipses whose semi-
29 angles are aligned with the eigenvectors. The semiangles are calculated
30 by
31

$$32 \begin{aligned} \epsilon_{12} &= \tan^{-1}(f\sigma/2(\lambda_1 - \lambda_2)) \\ \epsilon_{23} &= \tan^{-1}(f\sigma/2(\lambda_2 - \lambda_3)) \\ \epsilon_{13} &= \tan^{-1}(f\sigma/2(\lambda_1 - \lambda_3)) \\ \epsilon_{21} &= \epsilon_{12} \\ \epsilon_{32} &= \epsilon_{23} \\ \epsilon_{31} &= \epsilon_{13}, \end{aligned} \tag{2.3}$$

33 where ϵ_{ij} defines the semiaxis directed towards \mathbf{v}_j for the confidence region
34 of \mathbf{v}_i , and $f = \sqrt{2(F_{(2,n_f);(1-\alpha)})}$, being $F_{(2,n_f);(1-\alpha)}$ the $1 - \alpha$ quantile of
35 the F distribution with 2 and n_f degrees of freedom. For more details,
36 see Hext (1963).
37

38 In order to make the nomenclature consistent, $\eta_1 = \max(\epsilon_{12}, \epsilon_{13})$, and
39 $\zeta_1 = \min(\epsilon_{12}, \epsilon_{13})$. In the same way, we will rename the semiaxis $\eta_2, \zeta_2,$
40 η_3 and ζ_3 .
41
42
43
44

45 *2.3. Non-parametric bootstrap method*

46 The bootstrap method introduced by Constable and Tauxe (1990) is a non-
47 parametric bootstrap which consists of the following steps:
48
49
50
51
52
53
54

- 1
 - 2
 - 3
 - 4
 - 5
 - 6
 - 7
 - 8
 - 9
 - 10
 - 11
 - 12
 - 13
 - 14
 - 15
 - 16
 - 17
 - 18
 - 19
 - 20
 - 21
 - 22
 - 23
 - 24
 - 25
 - 26
 - 27
 - 28
 - 29
 - 30
 - 31
 - 32
 - 33
 - 34
 - 35
 - 36
 - 37
 - 38
 - 39
 - 40
 - 41
 - 42
 - 43
 - 44
 - 45
 - 46
 - 47
 - 48
 - 49
 - 50
 - 51
 - 52
 - 53
 - 54
 - 55
 - 56
 - 57
 - 58
 - 59
 - 60
 - 61
 - 62
 - 63
 - 64
 - 65
1. Compute the \mathbf{K}_j ($j = 1 \dots n$) from (1.3) and (1.2).¹
 2. Compute a pseudo-mean tensor $\bar{\mathbf{K}} = n^{-1} \sum_{i=1}^n \hat{\mathbf{K}}_i$, where $\hat{\mathbf{K}}_i$ ($i = 1 \dots n$) are randomly selected from the n initial tensors \mathbf{K}_j (re-sampling with replacement).
 3. Calculate the eigenparameters for $\bar{\mathbf{K}}$.
 4. Repeat N_b times the first three steps to obtain samples of the distributions of each of the eigenparameters.

We have used $N_b = 1000$ for the number of iterations of the method.

The mean eigenparameters will be calculated from $\bar{\mathbf{K}}_{\text{mean}} = N_b^{-1} \sum_{l=1}^{N_b} \bar{\mathbf{K}}_l$. And the confidence intervals for α confidence level are calculated assuming a normal distribution for each of the eigenvalues, and a Kent distribution for each of the eigenvectors, also called Fisher-Bingham 5 distribution (Kent, 1982). The details on the calculation of the confidence ellipse for the Kent distribution are given in Appendix A.

An important characteristic of the Kent distribution is that, when calculating the confidence ellipse from a set of vectors, the result changes if any of the vectors is exchanged by its opposite. However, if \mathbf{v} is an eigenvector, its opposite $-\mathbf{v}$ is an equally valid eigenvector. Because of this, the directions of the eigenvectors must be carefully chosen before calculating the corresponding confidence ellipse. In this paper, our selection criteria is the minimum angular distance between directions. That is, we choose, from the two antipodal eigenvectors, the one closer to the direction of the eigenvector of the mean susceptibility tensor.

2.4. Simulations

A total of 500 simulations have been run for each set of variables. The set of variables is constituted by the degree of anisotropy (P), the shape parameter (U), the standard deviation of the instrumental error distribution (σ) and the number of measurements (n).

Each variable constitutes a different piece of information in the final results. The standard deviation indicates how magnetically weak the data are, because σ is the ratio of the instrumental error to the mean susceptibility. The degree of anisotropy and the shape parameter indicate how anisotropically weak the data are. By increasing the number of measurements, the information about the instrumental error distribution and the statistical significance of the results are improved.

All the methods and simulations are implemented in R (free software programming language). The confidence level in all this study is set to 95%, being, therefore, $\alpha = 0.05$. The mean susceptibility λ_{mean} is taken as the unit of the susceptibility scale, so that the values of σ and the eigenvalues are dimensionless and to be understood as percentages of λ_{mean} . For the non-parametric bootstrap method, the repetition number N_b is set to 1000.

¹Usually the next step is normalize \mathbf{K}_j by its trace, but in this paper we do not normalize the tensor because the study is for only one sample measured n-times

1
2
3
4
5
6
7
8
9 **3. Results**

10 A set of simulations have been performed to show how the reliability of the
11 methods and their confidence intervals vary according to the ellipsoid param-
12 eters, the number of measurements and the instrumental error. The results are
13 displayed in seven figures, each of them containing eight graphs. In each figure
14 P and U are fixed and only the variable represented in the X-axes, either σ or
15 n , varies while the other one remains also fixed. For each value of the X-axis
16 variable, the plots in the eight graphs summarize the results of 500 simulations.
17

18 When σ varies, the value of n is fixed to $n = 20$, the threshold indicated
19 by Tauxe (1998) to satisfy a confidence level of 95% in the non-parametric
20 bootstrap. From these simulations we can determine a critical value, σ_c , that
21 indicates the maximum σ for which both methods satisfy a 95% confidence
22 level for $n = 20$. This σ_c is different for each set of values of P and U . When n
23 varies, the value of σ is fixed to a chosen value higher than σ_c . The reason to
24 run simulations varying n is to check if the reliability of the methods improves
25 when the number of measurements increases.
26

27 The chosen combinations of P and U correspond to different types of ellip-
28 soid. The values of P are 1.01 and 2, corresponding to a low anisotropy case
29 and a high anisotropy case, respectively. The values of U are 0, 0.9 and -0.9 ,
30 corresponding to a neutral, oblate and prolate ellipsoid, respectively, to study
31 the behavior of the two end-members, the case with two close eigenvalues and
32 the case with evenly spaced eigenvalues. We have not chosen the extreme values
33 $U = \pm 1$, when two eigenvalues are equal, because speaking of confidence ellipses
34 does not make sense in that case since the eigenvectors space would degenerate
35 to a plane.
36

37 Mathematically there is no difference between choosing oblate or prolate
38 ellipsoid, in both cases there are two eigenvalues very close to each other. Be-
39 cause of this, we have chosen an oblate ellipsoid ($U = 0.9$) for the case of low
40 anisotropy ($P = 1.01$) and a prolate ellipsoid ($U = -0.9$) for the case of high
41 anisotropy ($P = 2$).
42

43 All figures contain eight graphs distributed along two columns and four rows.
44 The graphs in the left column represent in the Y-axis the percentage of successful
45 results obtained by the two considered methods, with a dashed line indicating
46 the 95% success. The first graph represents the success percentage in the es-
47 timation of the AMS eigenvalues λ_1 , λ_2 and λ_3 . The second, third and fourth
48 graphs in the left side of the figure represent the success percentage in the es-
49 timation of the maximum, intermediate and minimum eigenvectors, \mathbf{v}_1 , \mathbf{v}_2 and
50 \mathbf{v}_3 respectively.
51

52 The graphs in the right column represent in the Y-axis the average size of
53 the confidence intervals obtained by the two methods for a 95% confidence level.
54 The first graph shows the average confidence intervals of the eigenvalues, $\Delta\lambda_1$,
55 $\Delta\lambda_2$ and $\Delta\lambda_3$. The second graph shows the mean semiaxes (semiangles) of the
56 confidence ellipse for the maximum eigenvalue, η_1 (major semiaxis), ζ_1 (minor
57 semiaxis), in radians. In the same way, the third and fourth graph show η_2 , ζ_2 ,
58 and η_3 , ζ_3 , for the intermediate and the minimum eigenvalue respectively.
59
60
61
62
63
64
65

In Figures 1, 2, and 3, the X-axis, in all graphs, represents σ , the standard deviation of the instrumental error distribution. In Figures 4, 5, 6, and 7, the X-axis, in all graphs, represents n , the number of measurements.

3.1. Influence of σ

Figure 1 summarizes the results of the experiment with a low anisotropy ($P = 1.01$) and neutral ellipsoid ($U = 0$) for $n = 20$. The differences between eigenvalues are 0.01, 1% of λ_{mean} . The value of σ_c , estimated from the graphs in the left column, is 0.005. This value of σ_c means that an instrumental error higher than 0.5% of λ_{mean} will provide a no reliable AMS ellipsoid for this set of values of P , U and n .

Figure 2 corresponds to the example of low anisotropy and oblate ellipsoid for $n = 20$. The difference between eigenvalues are $\lambda_1 - \lambda_2 = 5 \cdot 10^{-4}$ [SI] and $\lambda_2 - \lambda_3 = 9.4 \cdot 10^{-3}$ [SI]. In this case, the value of σ_c is less than 0.001. The LPA method reaches a confidence level of 95% for the eigenvalues and the eigenvector associated to the distinct eigenvalue (λ_3) for $\sigma = 0.01$, but not for the eigenvectors associated to the other eigenvalues. The NPB method only reaches a 95% confidence level for the eigenvalues for $\sigma = 0.001$.

Figure 3 display the results for a high anisotropy ($P = 2$) and neutral ellipsoid ($U = 0$) for $n = 20$. In this case, the value of σ_c is 0.2 and the differences between eigenvalues is 0.7.

The Figures 1, 2 and 3 show that σ has to be smaller than the differences between eigenvalues to be able to distinguish the eigenvalues and to make a good interpretation of the principal directions. The range of reliability for both methods decreases (smaller σ_c) as the absolute value of the shape parameter increases and the anisotropy degree decreases. The results of the LPA and the NPB methods are much closer for $\sigma \leq \sigma_c$, both in the reliability and in the size of the confidence intervals. When the value of σ_c is exceeded, the negative slope in the eigenvectors reliability graphs of the LPA method is higher than the one of the NPB method, but the sizes of the NPB confidence intervals are much bigger, quickly approaching 90° . For the eigenvalues, the reverse behavior is observed, being the LPA method more reliable, without a big difference in the sizes of the confidence intervals, though. The case for $P = 2$, $U = -0.9$ and $n = 20$ is not shown in this paper because the trend is similar to the Figure 2, with a value of $\sigma_c = 0.05$.

3.2. Influence of n

In figures 4,5, 6 and 7 we show how the reliability of the methods and the confidence intervals change when n increases for fixed values of P , U and σ . These graphs demonstrate that, by increasing the number of measurements, we can improve the reliability and minimize the AMS confidence intervals around half.

Figure 4 shows the case of low anisotropy and neutral ellipsoid for a value of $\sigma = 0.02$, four times the value of σ_c . We can see that the NPB method needs $n \geq 50$ to reach a 95% confidence and the LPA method, $n \geq 100$. Figure 5, the

1
2
3
4
5
6
7
8
9
10
11
12
13
14
15
16
17
18
19
20
21
22
23
24
25
26
27
28
29
30
31
32
33
34
35
36
37
38
39
40
41
42
43
44
45
46
47
48
49
50
51
52
53
54
55
56
57
58
59
60
61
62
63
64
65

case of high anisotropy and neutral ellipsoid for a value of $\sigma = 1$, five times the value of σ_c , shows a critical value of $n = 50$ for both methods. Figure 6 reflects the case of high anisotropy and prolate ellipsoid for a value of $\sigma = 0.2$, four times the value of σ_c . In this figure, the critical value of n for the eigenvalues is $n = 50$ for both methods, but for the eigenvectors, the NPB method needs $n = 50$ and the LPA method needs more than one hundred measurements.

In the figure 7 we have simulated a case with $P = 1.01$, $U = 0.9$ and $\sigma = 0.01$, ten times the value of σ_c . A mineral with similar values of P and U is the quartz with $P = 1.01$ and $U = 1$ (Tarling and Hrouda,1993). For quartz, with $k_{\text{bulk}} \sim 13 \cdot 10^{-6}$ [SI], a value of $\sigma = 0.01$ would translate to an instrumental error of $1 \cdot 10^{-7}$ [SI]. This value can correspond to the total instrumental error for AGICO Instruments, since their sensitivity is in the range of 10^{-8} [SI] (Hrouda, 2011) and the total error is at least one order of magnitude larger than the sensitivity (Biedermann et al., 2013). For this case, only the LPA method can determine the eigenvalues with a 95% confidence level for the whole range of n (from 8 to 100). The NPB method cannot reach a 95% confidence level (for the eigenvalues) even with one hundred measurements. For the eigenvectors, no method can reach a 95% confidence level for the eigenvectors associated to the closest eigenvalues (Hall et al., 2009).

4. Discussion and conclusions

In this paper we have explored the well-resolved region for which the Linear Perturbation Analysis by Hext (1963) and the non-parametric bootstrap method proposed by Constable and Tauxe (1990) are reliable at a 95% confidence level. For that, we have performed simulations varying the ellipsoid parameters, P and U , the number of measurements n and the standard deviation of the instrumental error distribution, σ , taking as susceptibility unit the mean susceptibility λ_{mean} .

We have observed that the reliability of both methods depends on the ratio of instrumental error to mean susceptibility (magnetically weak samples) and the spacing of eigenvalues (anisotropically weak samples). For both methods there exists a maximum value of σ , named here critical value σ_c , for which the methods are reliable. This value of σ_c increases as the difference between eigenvalues does. That is, the value of σ_c is higher when the anisotropy degree increases and the shape parameter decreases. In order to reach the confidence level of 95% in both methods, the value of σ has to be smaller than the minimum difference between eigenvalues, at least for $n \lesssim 20$.

For fixed P and U , the confidence intervals are similar for both methods when they both are in their well-resolved region. When outside the well-resolved region, the behavior of both methods is different for the estimation of eigenvalues and their eigenvectors. For the eigenvalues, the success rate obtained by the LPA method is always higher than the one of the non-parametric bootstrap method, although the sizes of the eigenvalues errors of the LPA method are not much bigger. For the eigenvectors, the reverse is true. However, there is a big difference between the size of the errors (the semiangles obtained by the NPB

1
2
3
4
5
6
7
8
9 method quickly overtake the value of 50°). Simulations reveal that when the
10 methods are not reliable for a certain experimental setup (n, σ) , the reliability
11 region may be reached by sufficiently increasing n , resulting in considerably
12 better accuracy too.

13 From these results we can suggest that when the eigenparameters are calcu-
14 lated by the two methods and the results are similar, then, they are in their well-
15 resolved region and the results are reliable. But if there is a difference, the LPA
16 method tends to be more reliable for the eigenvalues and the non-parametric
17 bootstrap method for the eigenvectors, although the confidence ellipses may be
18 too large for the results to be useful.

19 The current study can be used as an estimator of the measuring protocol for
20 the evaluation of single crystal properties, where a previous estimation of the pa-
21 rameters $(P, U, \lambda_{\text{mean}})$ is available from theoretical calculations or preliminary
22 measurements. From this previous estimation we can get an approximation of
23 the spacing between eigenvalues $(\Delta\lambda)$. Since the instrumental error distribution
24 (and its σ) is part of the empirical method and cannot be changed significantly,
25 the required number of measurements can be estimated before the actual mea-
26 surement work is carried out. If $\sigma \leq \Delta\lambda/2$, $n = 20$ is enough to obtain reliable
27 parameters. If $\sigma \sim \Delta\lambda$ it is necessary a value of $n = 50$. If $\sigma \geq 2\Delta\lambda$, n will
28 reach unpractical values over one hundred measurements. The results presented
29 in this work show the importance of the instrumental error distribution. This
30 includes together with the technical instrumental sensitivity, additional sources
31 of systematic errors related to the particular instrument and its location. It
32 would be recommended for very precise determinations of AMS properties the
33 evaluation of σ for each laboratory.
34
35
36

37 **Acknowledgment**

38
39 Authors are warmly grateful to G. Horcajada for helping with the develop-
40 ment of the software and discussion. This paper has benefited significantly from
41 two anonymous reviewer comments and Editor M. Jackson. Also Prof. A. M.
42 Hirt is acknowledged for fruitful discussion. This work is supported by Project
43 no CGL2011-24790 from Spanish Ministry of Economy and Competitiveness to
44 SGS and a Ramon y Cajal contract to FMH.
45
46

47 **Appendix A. Confidence ellipse calculation for the Kent distribution**

48 According to Kent (1982), a $1 - \alpha$ confidence ellipse can be obtained for
49 the mean value $\bar{\mathbf{x}}$ of a set of vectors \mathbf{x}_i , with $i = 1 \dots N_b$, that follow a Kent
50 distribution. To obtain the ellipse parameters, the following steps are followed:
51

- 52 · calculate the mean vector $\bar{\mathbf{x}} = N_b^{-1} \sum \mathbf{x}_i$;
- 53
- 54 · calculate the dispersion matrix $\mathbf{S} = N_b^{-1} \sum \mathbf{x}_i \mathbf{x}_i^T$;
- 55
- 56
- 57
- 58

- 1
2
3
4
5
6
7
8
9 · choose a rotation matrix \mathbf{H} that rotates $\bar{\mathbf{x}}$ to the north polar axis, i.e.

$$10 \quad \mathbf{H} = \begin{pmatrix} \cos(\theta) \cos(\phi) & -\sin(\phi) & \sin(\theta) \cos(\phi) \\ \cos(\theta) \sin(\phi) & \cos(\phi) & \sin(\theta) \sin(\phi) \\ -\sin(\theta) & 0 & \cos(\theta) \end{pmatrix},$$

14 where θ and ϕ are the polar coordinates of $\bar{\mathbf{x}}$;

- 15
16 · calculate the matrix $\mathbf{B} = \mathbf{H}^T \mathbf{S} \mathbf{H}$;
17
18 · choose a rotation matrix \mathbf{W} about the north pole to diagonalize the upper
19 2-by-2 submatrix of \mathbf{B} ,

$$20 \quad \mathbf{W} = \begin{pmatrix} \cos(\psi) & -\sin(\psi) & 0 \\ \sin(\psi) & \cos(\psi) & 0 \\ 0 & 0 & 1 \end{pmatrix};$$

- 21
22 · calculate the orientation matrix $\mathbf{\Gamma} = \mathbf{H} \mathbf{W}$, which is also a rotation;
23
24 · use $\mathbf{\Gamma}$ to transform the original vectors to the population standard frame
25 of reference: $\mathbf{x}_i^* = \mathbf{\Gamma}^T \mathbf{x}_i$;
26
27 · in this standard frame of reference, with coordinates (x_1^*, x_2^*, x_3^*) , the con-
28 fidence ellipse's equation takes the form

$$29 \quad N_b \mu^2 \left(\frac{x_1^{*2}}{\sigma_1^2} + \frac{x_2^{*2}}{\sigma_2^2} \right) < \chi_{2;\alpha}^2, \quad (4.1)$$

30 where $\chi_{2;\alpha}^2$ denotes the upper α critical value of the chi-squared distribu-
31 tion with 2 degrees of freedom, and

$$32 \quad \mu = N_b^{-1} \sum \mathbf{x}_{i3}^*, \quad \sigma_1^2 = N_b^{-1} \sum \mathbf{x}_{i1}^{*2}, \quad \sigma_2^2 = N_b^{-1} \sum \mathbf{x}_{i2}^{*2};$$

- 33
34 · from (4.1), the major and minor semiaxes of the confidence ellipse are
35 $\eta = \arcsin \left(\sqrt{\frac{\sigma_1 \chi_{2;\alpha}^2}{N_b \mu^2}} \right)$ and $\zeta = \arcsin \left(\sqrt{\frac{\sigma_2 \chi_{2;\alpha}^2}{N_b \mu^2}} \right)$, while the directions of
36 the semiaxes are obtained from the two first columns of the orientation
37 matrix $\mathbf{\Gamma}$.
38

39 References

- 40 Biedermann, A.R., Lowrie, W., Hirt, A.M., 2013. A method for improving the
41 measurement of low-field magnetic susceptibility anisotropy in weak samples.
42 Journal of Applied Geophysics 88, 122–130.
43
44 Borradaile, G., Henry, B., 1997. Tectonic applications of magnetic susceptibility
45 and its anisotropy. Earth-Science Reviews 42, 49–93.
46
47
48
49
50
51
52
53
54
55
56
57
58
59
60
61
62
63
64
65

- 1
2
3
4
5
6
7
8
9 Borradaile, G.J., 2003. Statistics of earth science data: their distribution in
10 time, space and orientation. Springer.
- 11
12 Borradaile, G.J., Jackson, M., 2010. Structural geology, petrofabrics and mag-
13 netic fabrics (ams, aarm, airm). *Journal of Structural Geology* 32, 1519–1551.
- 14
15 Borradaile, G.J., Stupavsky, M., Metsaranta, D.A., 2008. Induced magnetiza-
16 tion of magnetite-titanomagnetite in alternating fields ranging from 400 a/m
17 to 80,000 a/m; low-field susceptibility (100–400 a/m) and beyond. *Pure and*
18 *Applied Geophysics* 165, 1411–1433.
- 19
20 Cañón-Tapia, E., Walker, G.P., Herrero-Bervera, E., 1995. Magnetic fabric and
21 flow direction in basaltic pahoehoe lava of xitle volcano, mexico. *Journal of*
22 *volcanology and geothermal research* 65, 249–263.
- 23
24 Constable, C., Tauxe, L., 1990. The bootstrap for magnetic susceptibility ten-
25 sors. *Journal of Geophysical Research: Solid Earth (1978–2012)* 95, 8383–
26 8395.
- 27
28 Davison, A.C., 1997. Bootstrap methods and their application. volume 1. Cam-
29 bridge university press.
- 30
31 Dunlop, D.J., Özdemir, Ö., 2001. Rock magnetism: fundamentals and frontiers.
32 volume 3. Cambridge University Press.
- 33
34 Ernst, R.E., Baragar, W., 1992. Evidence from magnetic fabric for the flow
35 pattern of magma in the mackenzie giant radiating dyke swarm. *Nature* 356,
36 511–513.
- 37
38 Hall, P., L, Y.K., P, B.U., P, D., 2009. Tie-respecting bootstrap methods for
39 estimating distributions of sets and functions of eigenvalues. *Bernoulli* 15,
40 380–401.
- 41
42 Hamilton, N., Rees, A., 1970. The use of magnetic fabric in paleocurrent esti-
43 mation. *Palaeogeophysics* , 445–464.
- 44
45 Hext, G.R., 1963. The estimation of second-order tensors, with related tests
46 and designs. *Biometrika* 50, 353–373.
- 47
48 Hrouda, F., 1993. Theoretical models of magnetic anisotropy to strain relation-
49 ship revisited. *Physics of the Earth and Planetary Interiors* 77, 237–249.
- 50
51 Hrouda, F., 2002. Low-field variation of magnetic susceptibility and its effect
52 on the anisotropy of magnetic susceptibility of rocks. *Geophysical Journal*
53 *International* 150, 715–723.
- 54
55 Hrouda, F., Pokorný, J., 2011. Extremely high demands for measurement accu-
56 racy in precise determination of frequency-dependent magnetic susceptibility
57 of rocks and soils. *Studia Geophysica et Geodaetica* 55, 667–681.

- 1
2
3
4
5
6
7
8
9 Jelinek, V., 1977. The statistical theory of measuring anisotropy of magnetic
10 susceptibility of rocks and its application. *Geofyzika*, Brno 87.
11
12 Jelínek, V., 1978. Statistical processing of anisotropy of magnetic susceptibility
13 measured on groups of specimens. *Studia geophysica et geodaetica* 22, 50–62.
14
15 Jelinek, V., 1981. Characterization of the magnetic fabric of rocks. *Tectono-*
16 *physics* 79, T63–T67.
17
18 Kent, J.T., 1982. The fisher-bingham distribution on the sphere. *Journal of the*
19 *Royal Statistical Society. Series B (Methodological)* , 71–80.
20
21 Kodama, K.P., 1995. Magnetic fabrics. *Reviews of Geophysics* 33, 129–135.
22
23 Nagata, T., 1961. *Rock magnetism*. Maruzen Company Tokyo.
24
25 Owens, W., 2000a. Statistical analysis of normalized and unnormalized second-
26 rank tensor data, with application to measurements of anisotropy of magnetic
27 susceptibility. *Geophysical research letters* 27, 2985–2988.
28
29 Owens, W., 2000b. Statistical applications to second-rank tensors in magnetic
30 fabric analysis. *Geophysical Journal International* 142, 527–538.
31
32 Rochette, P., Jackson, M., Aubourg, C., 1992. Rock magnetism and the inter-
33 pretation of anisotropy of magnetic susceptibility. *Reviews of Geophysics* 30,
34 209–226.
35
36 Schmidt, V., Günther, D., Hirt, A.M., 2006. Magnetic anisotropy of calcite at
37 room-temperature. *Tectonophysics* 418, 63–73.
38
39 Tarling, D., Hrouda, F., 1993. *Magnetic anisotropy of rocks*. Springer.
40
41 Tauxe, L., 1998. *Paleomagnetic principles and practice*. Number 17 in *Modern*
42 *approaches in geophysics*, Kluwer Academic Publishers, Dordrecht ; Boston.
43
44 Tauxe, L., 2010. *Essentials of paleomagnetism*. University of California Press,
45 Berkeley.
46
47 Werner, T., 1997. Experimental designs for determination of the anisotropy of
48 remanence-test of the efficiency of least-square and bootstrap methods applied
49 to metamorphic rocks from southern poland. *Physics and Chemistry of the*
50 *Earth* 22, 131–136.
51
52
53
54
55
56
57
58
59
60
61
62
63
64
65

1
2
3
4
5
6
7
8
9
10
11
12
13
14
15
16
17
18
19
20
21
22
23
24
25
26
27
28
29
30
31
32
33
34
35
36
37
38
39
40
41
42
43
44
45
46
47
48
49
50
51
52
53
54
55
56
57
58
59
60
61
62
63
64
65

U = 0, P = 1.01, n = 20

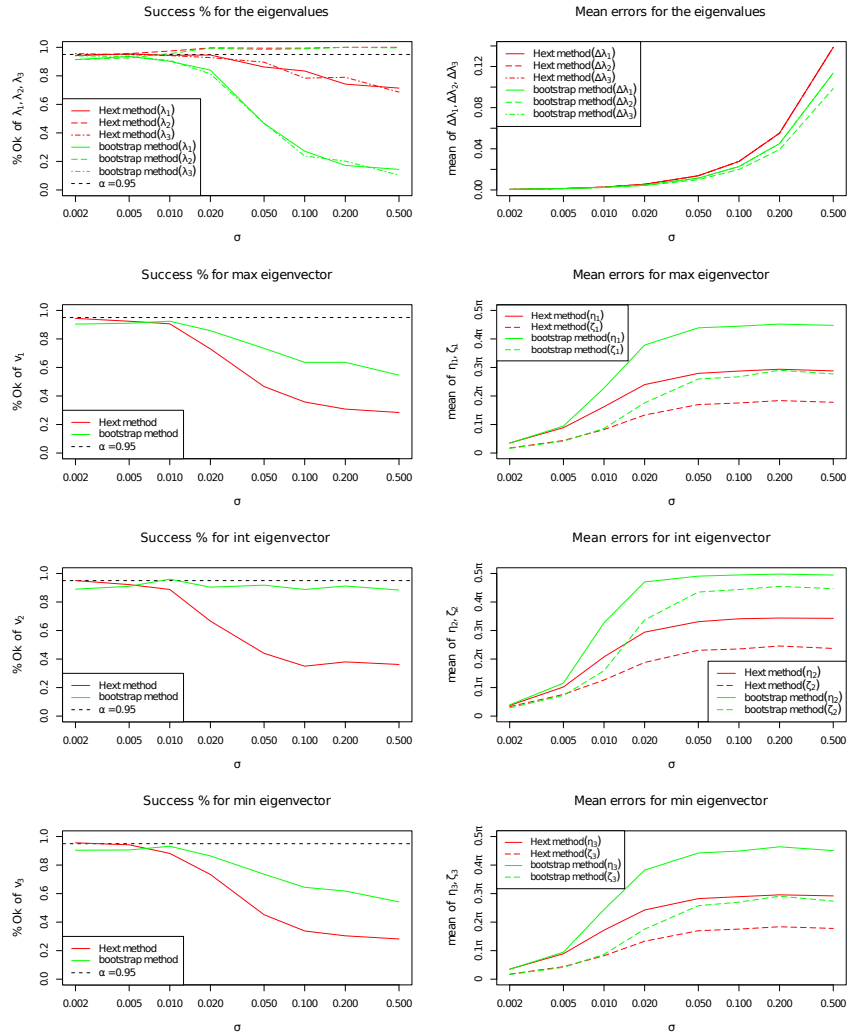


Figure 1: Average mean errors of the eigenparameters and their reliability for P=1.01, U=0, n=20

1
2
3
4
5
6
7
8
9
10
11
12
13
14
15
16
17
18
19
20
21
22
23
24
25
26
27
28
29
30
31
32
33
34
35
36
37
38
39
40
41
42
43
44
45
46
47
48
49
50
51
52
53
54
55
56
57
58
59
60
61
62
63
64
65

U = 0.9, P = 1.01, n = 20

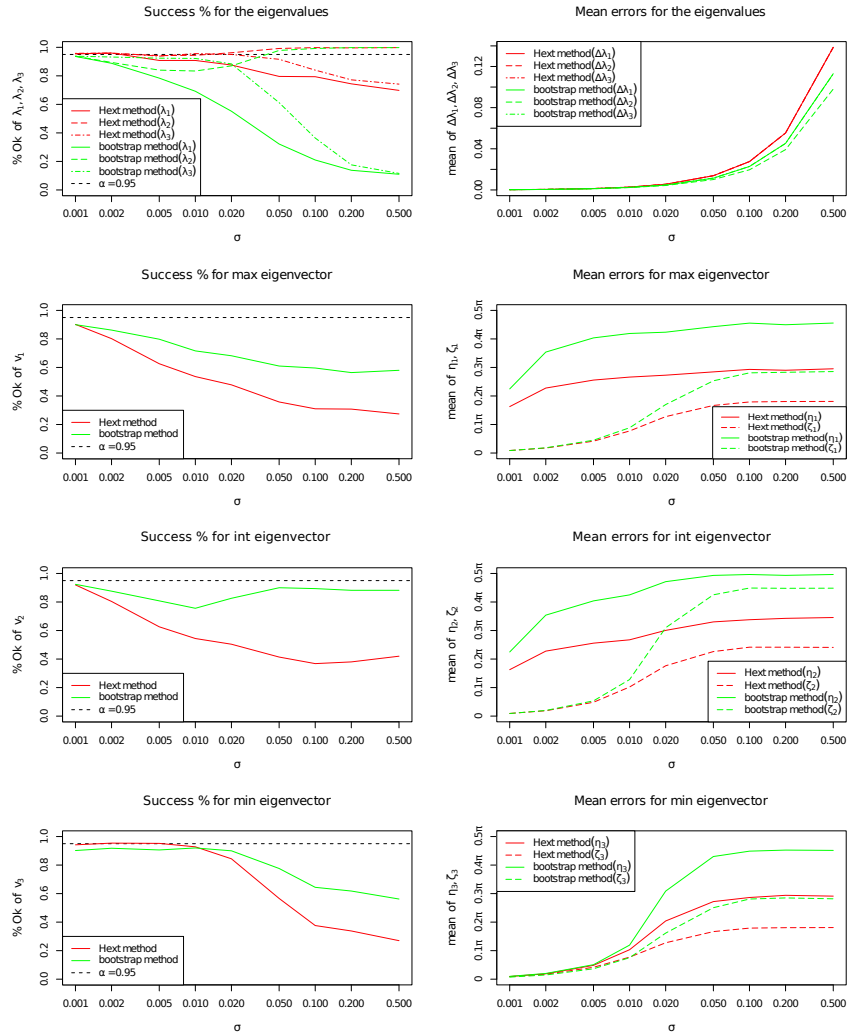


Figure 2: Average mean errors of the eigenparameters and their reliability for P=1.01, U=0.9, n=20

1
2
3
4
5
6
7
8
9
10
11
12
13
14
15
16
17
18
19
20
21
22
23
24
25
26
27
28
29
30
31
32
33
34
35
36
37
38
39
40
41
42
43
44
45
46
47
48
49
50
51
52
53
54
55
56
57
58
59
60
61
62
63
64
65

U = 0, P = 2, n = 20

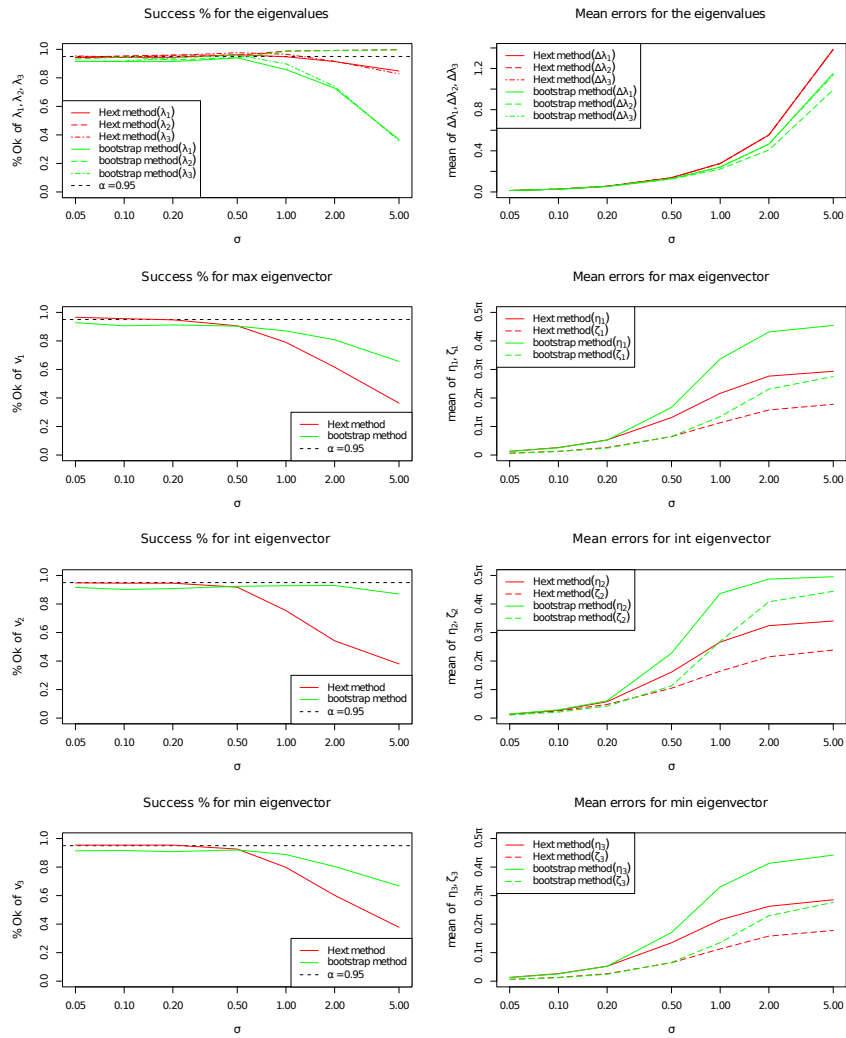


Figure 3: Average mean errors of the eigenparameters and their reliability for P=2, U=0, n=20

1
2
3
4
5
6
7
8
9
10
11
12
13
14
15
16
17
18
19
20
21
22
23
24
25
26
27
28
29
30
31
32
33
34
35
36
37
38
39
40
41
42
43
44
45
46
47
48
49
50
51
52
53
54
55
56
57
58
59
60
61
62
63
64
65

U = 0, P = 1.01, $\sigma = 0.02$

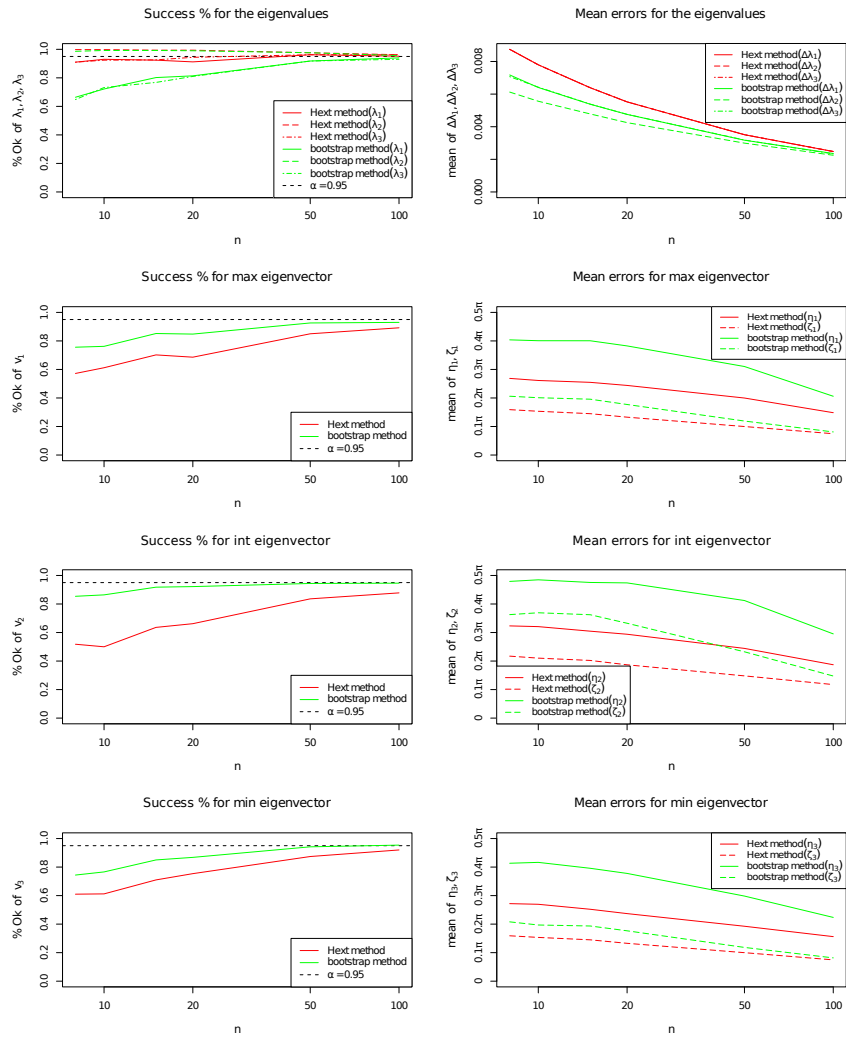


Figure 4: Average mean errors of the eigenparameters and their reliability for $P=1.01, U=0, \sigma = 0.02$

1
2
3
4
5
6
7
8
9
10
11
12
13
14
15
16
17
18
19
20
21
22
23
24
25
26
27
28
29
30
31
32
33
34
35
36
37
38
39
40
41
42
43
44
45
46
47
48
49
50
51
52
53
54
55
56
57
58
59
60
61
62
63
64
65

U = 0, P = 2, $\sigma = 1$

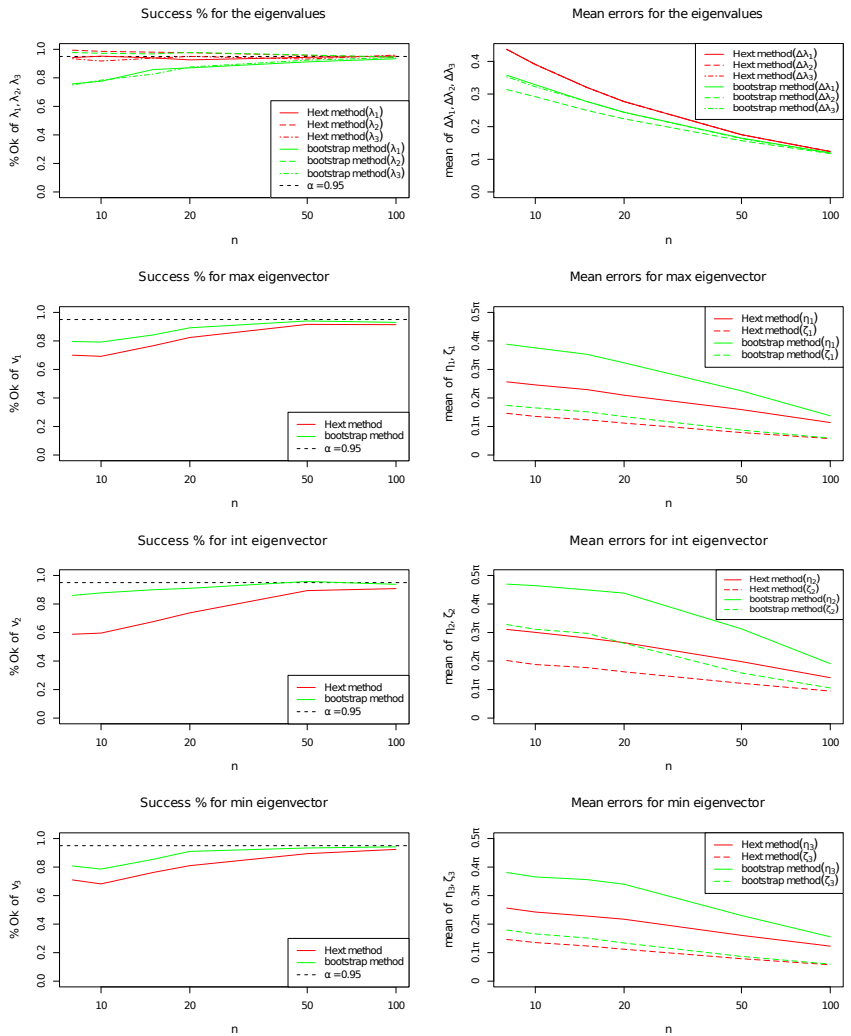


Figure 5: Average mean errors of the eigenparameters and their reliability for P=2, U=0, $\sigma = 1$

1
2
3
4
5
6
7
8
9
10
11
12
13
14
15
16
17
18
19
20
21
22
23
24
25
26
27
28
29
30
31
32
33
34
35
36
37
38
39
40
41
42
43
44
45
46
47
48
49
50
51
52
53
54
55
56
57
58
59
60
61
62
63
64
65

$U = -0.9, P = 2, \sigma = 0.2$

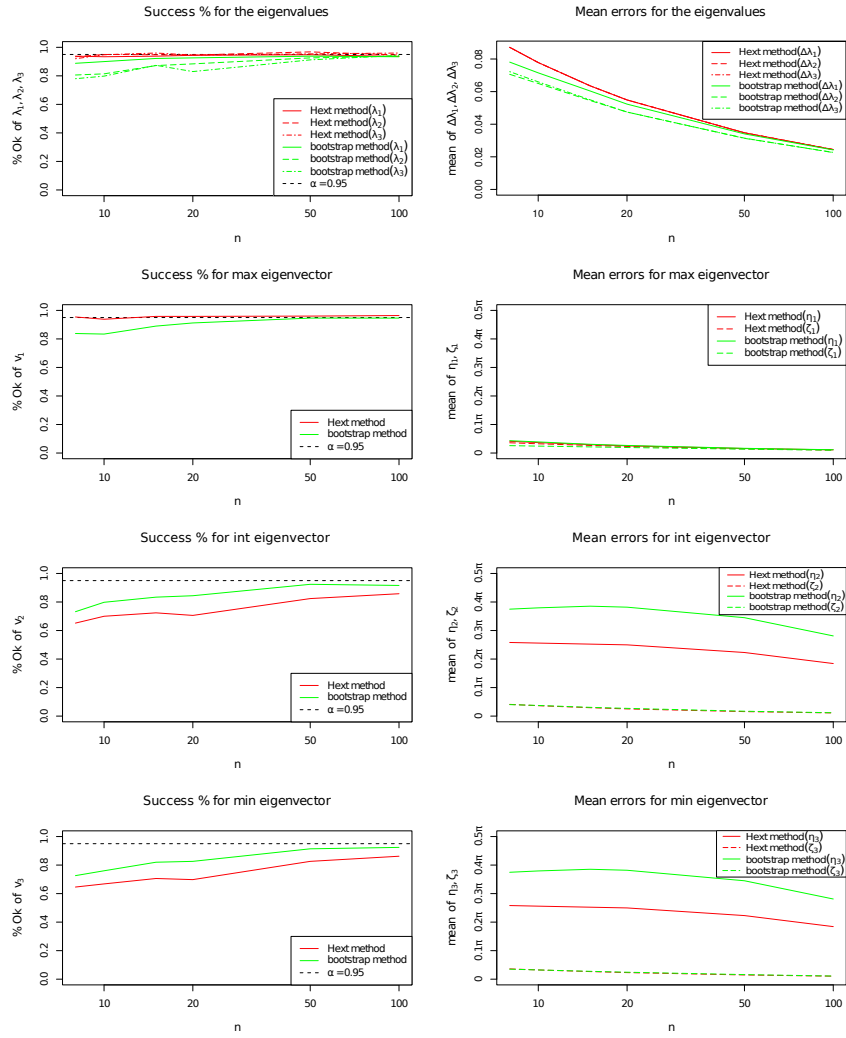


Figure 6: Average mean errors of the eigenparameters and their reliability for $P=2, U=-0.9, \sigma = 0.2$

1
2
3
4
5
6
7
8
9
10
11
12
13
14
15
16
17
18
19
20
21
22
23
24
25
26
27
28
29
30
31
32
33
34
35
36
37
38
39
40
41
42
43
44
45
46
47
48
49
50
51
52
53
54
55
56
57
58
59
60
61
62
63
64
65

U = 0.9, P = 1.01, $\sigma = 0.01$

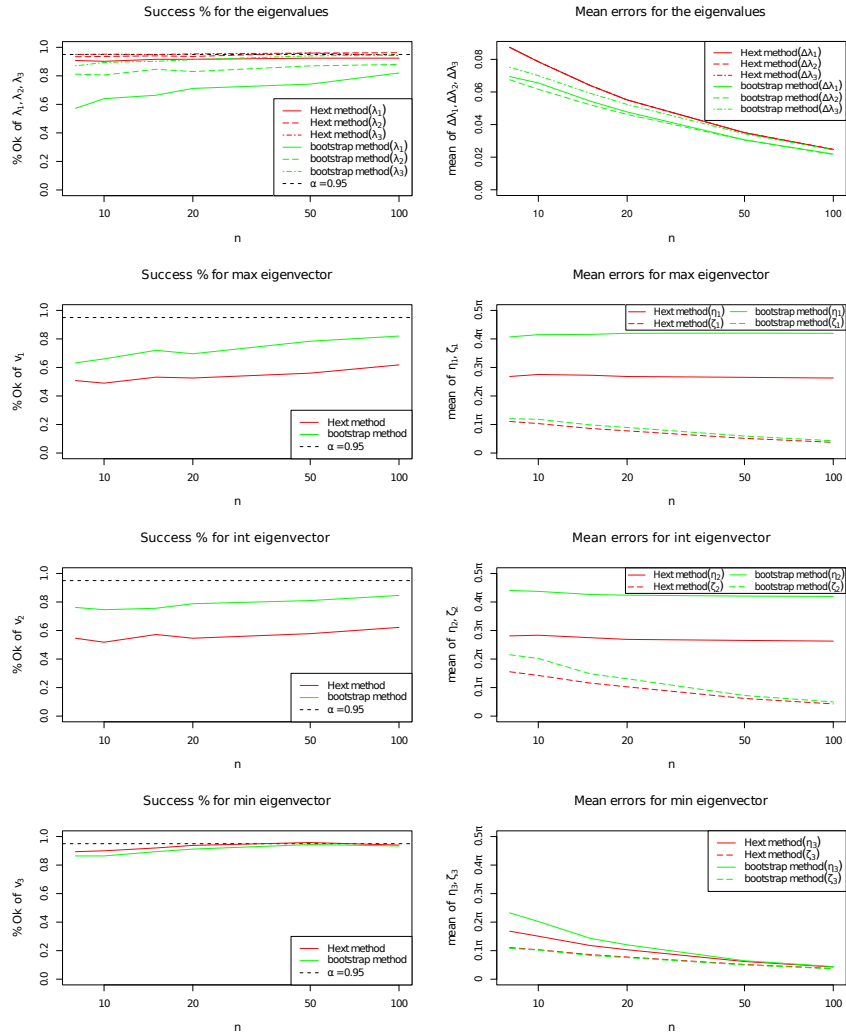
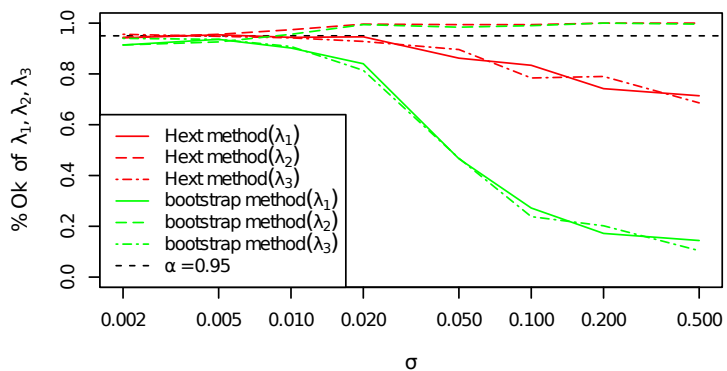


Figure 7: Average mean errors of the eigenparameters and their reliability for $P=1.01$, $U=0.9$, $\sigma = 0.01$

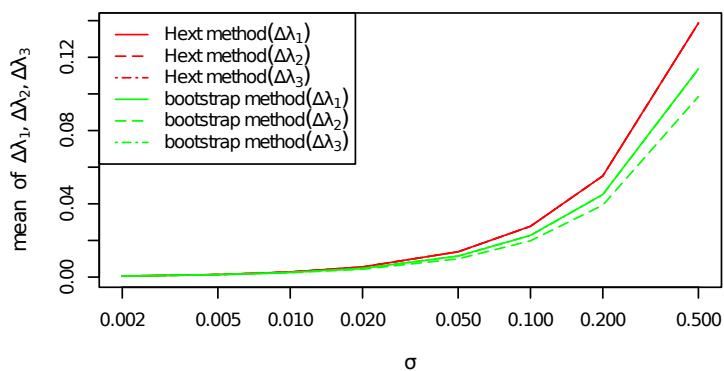
Figure 1

$U=0, P=1.01, n=20$

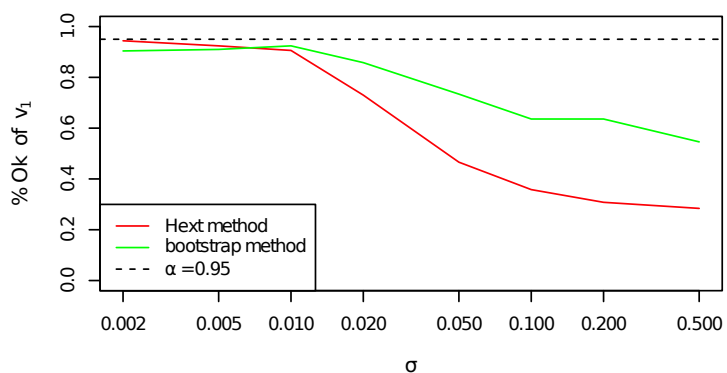
Success % for the eigenvalues



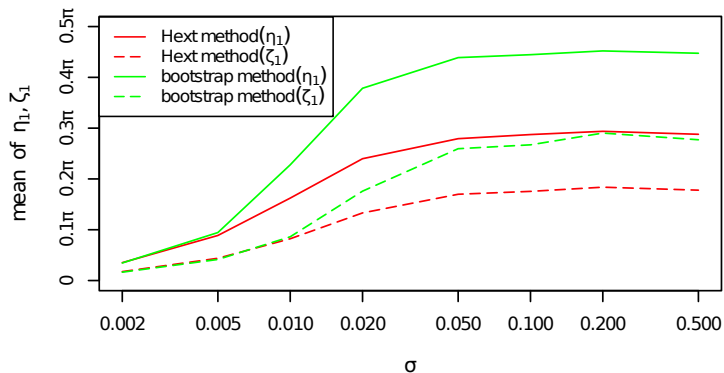
Mean errors for the eigenvalues



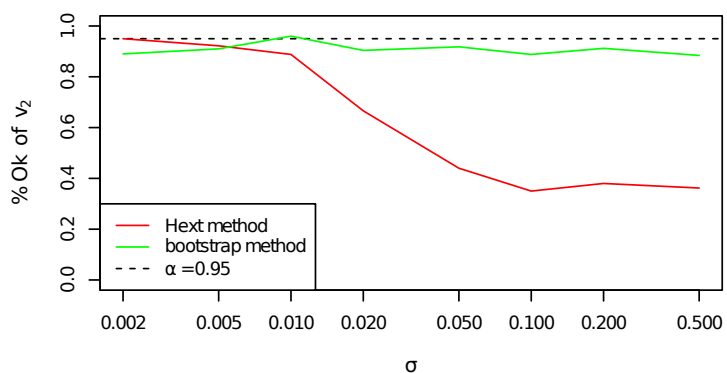
Success % for max eigenvector



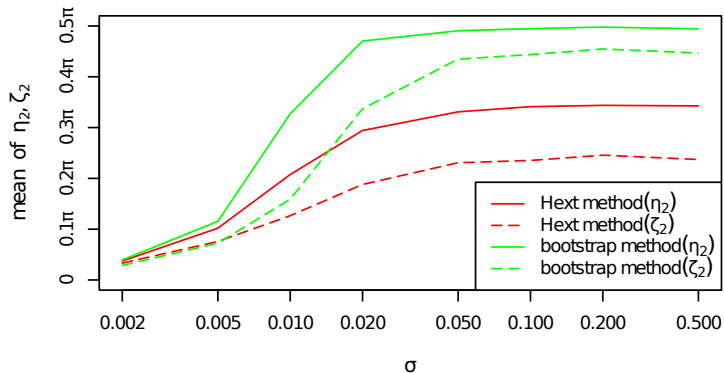
Mean errors for max eigenvector



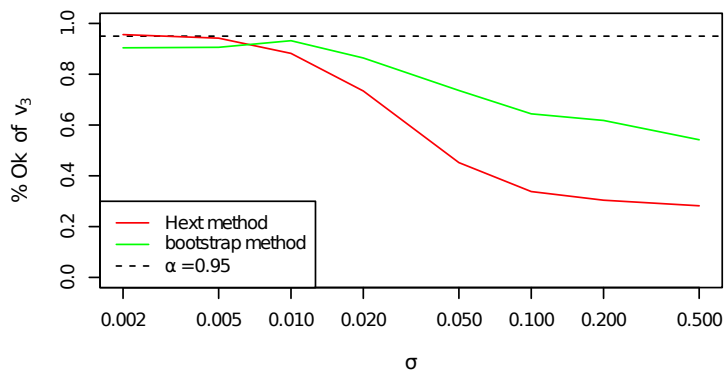
Success % for int eigenvector



Mean errors for int eigenvector



Success % for min eigenvector



Mean errors for min eigenvector

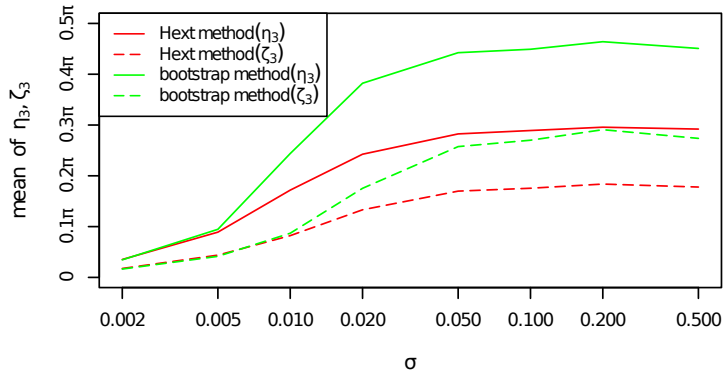
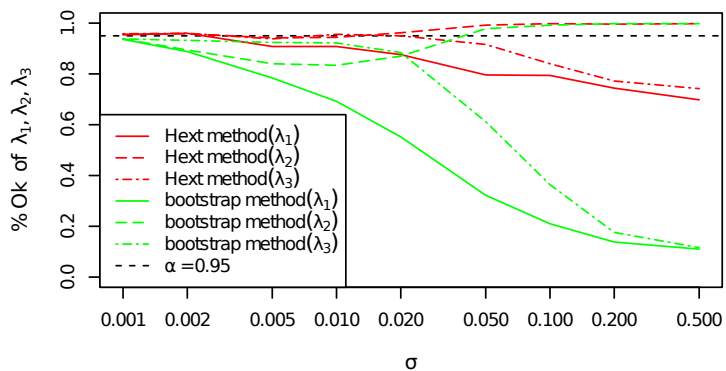


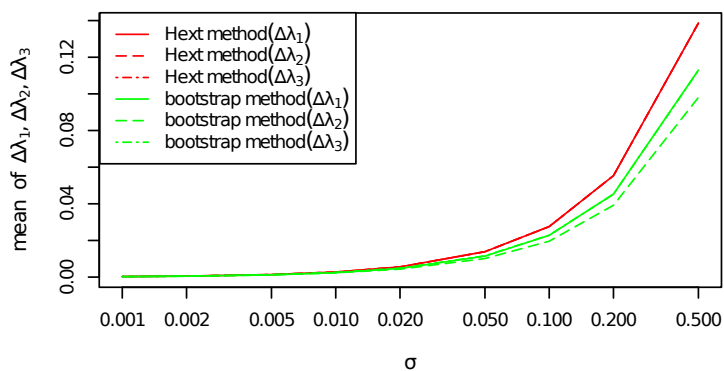
Figure 2

U = 0.9, P = 1.01, n = 20

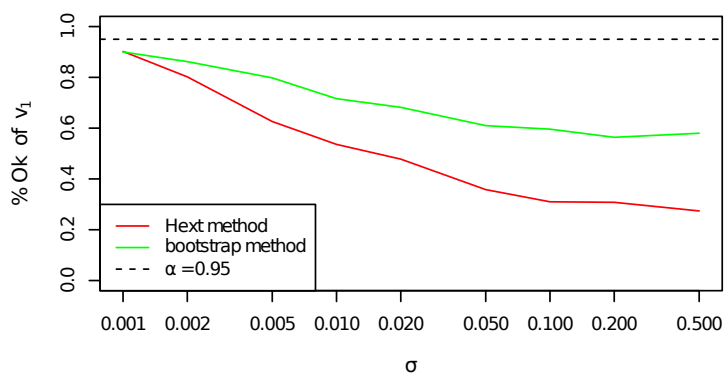
Success % for the eigenvalues



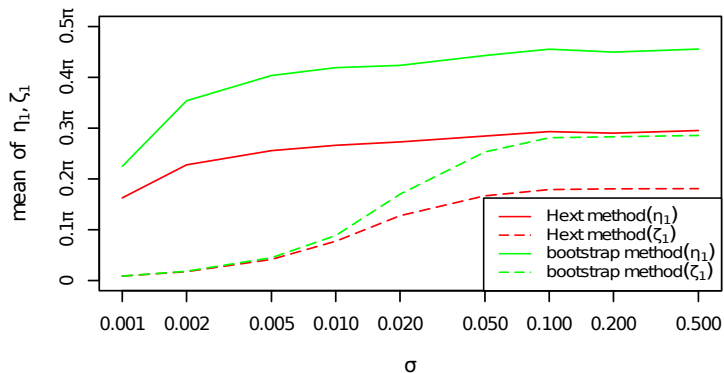
Mean errors for the eigenvalues



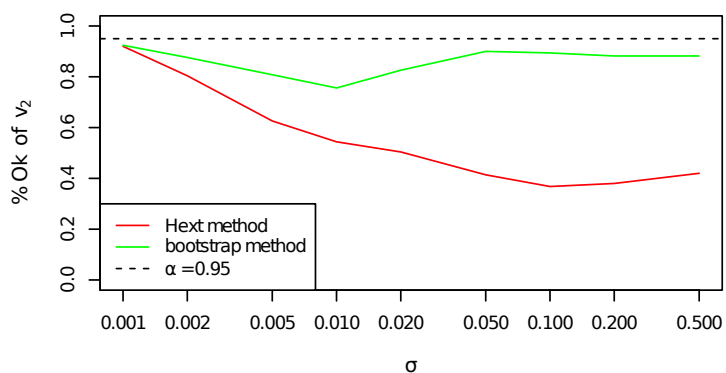
Success % for max eigenvector



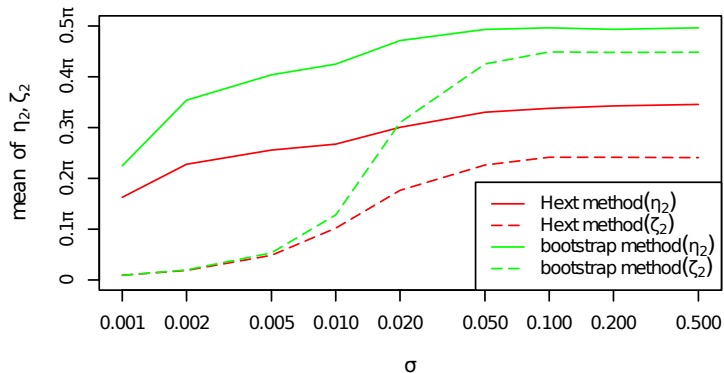
Mean errors for max eigenvector



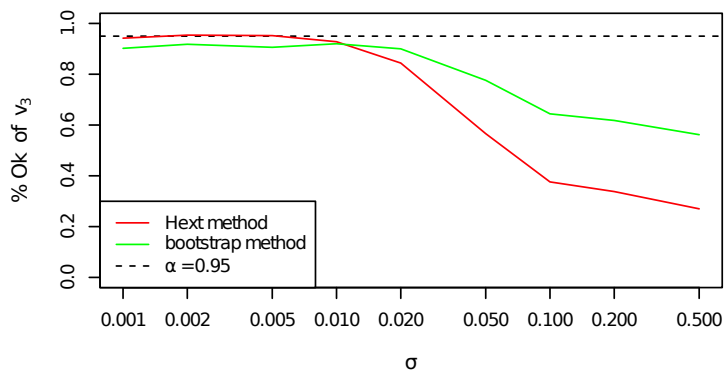
Success % for int eigenvector



Mean errors for int eigenvector



Success % for min eigenvector



Mean errors for min eigenvector

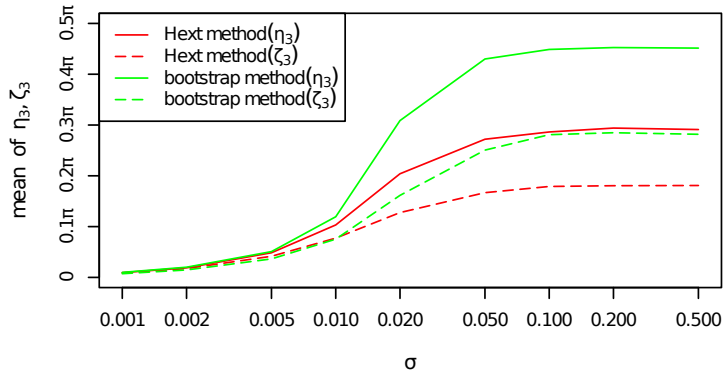
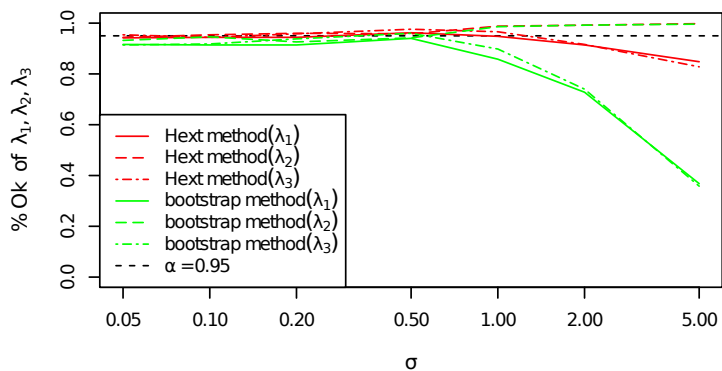


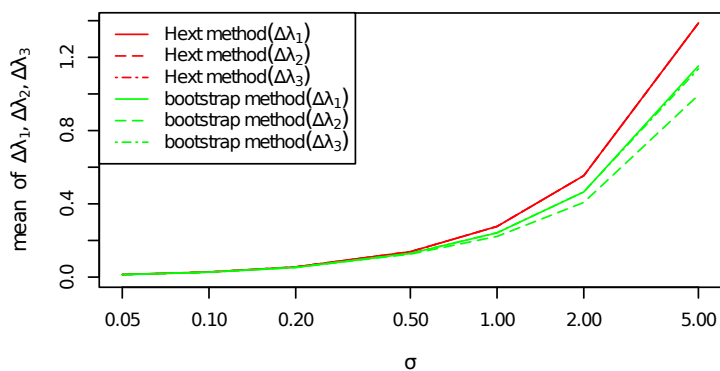
Figure 3

U=0, P=2, n=20

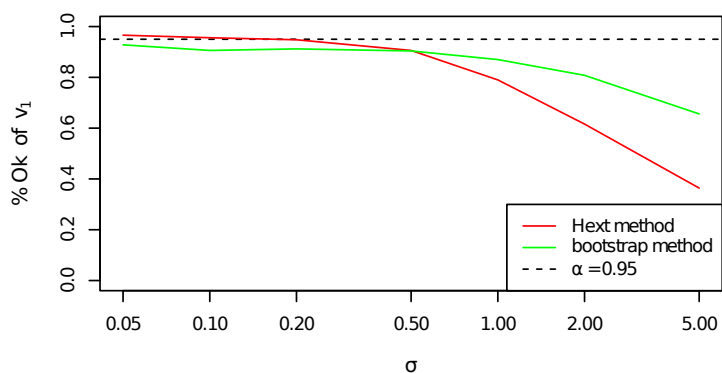
Success % for the eigenvalues



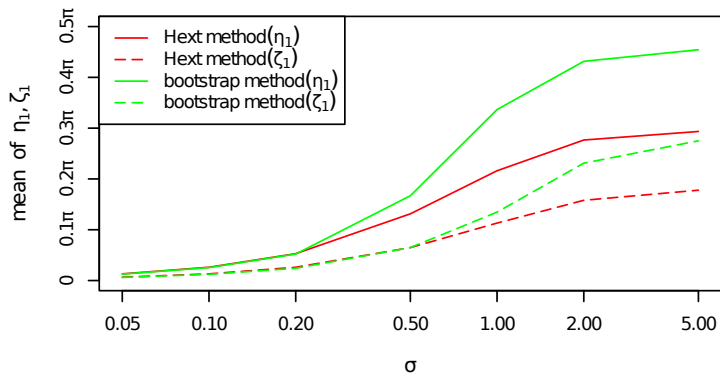
Mean errors for the eigenvalues



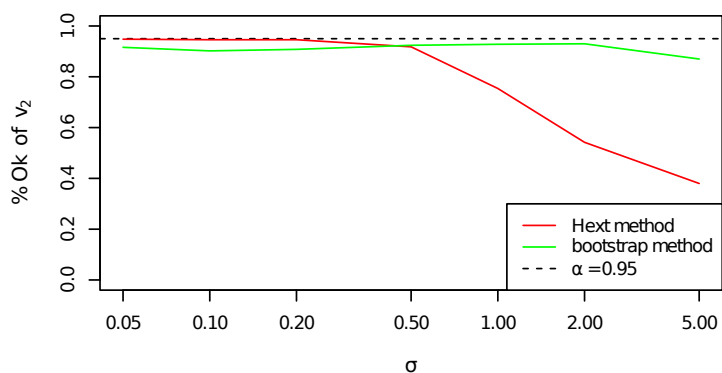
Success % for max eigenvector



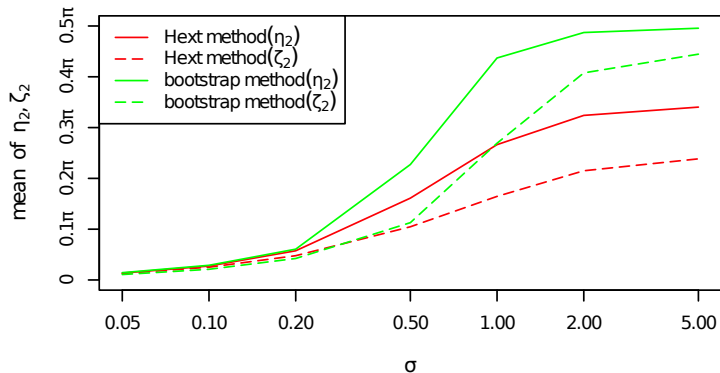
Mean errors for max eigenvector



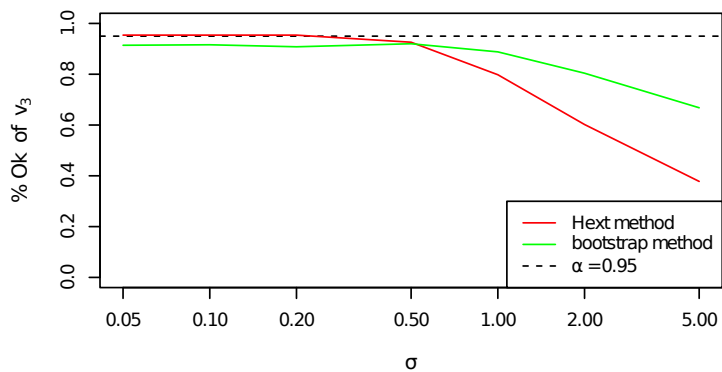
Success % for int eigenvector



Mean errors for int eigenvector



Success % for min eigenvector



Mean errors for min eigenvector

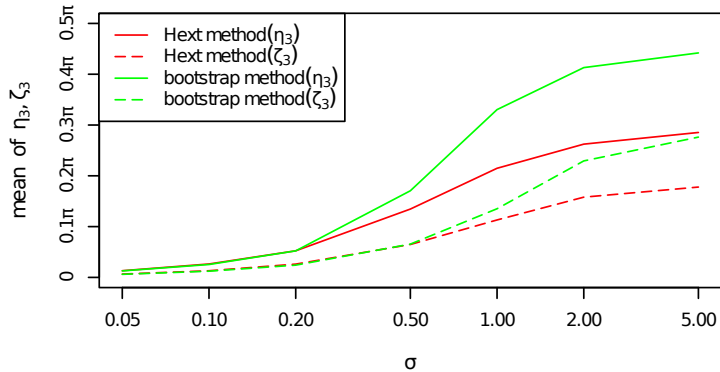
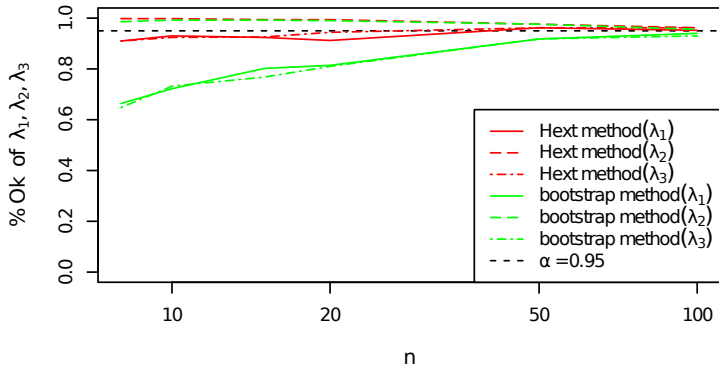


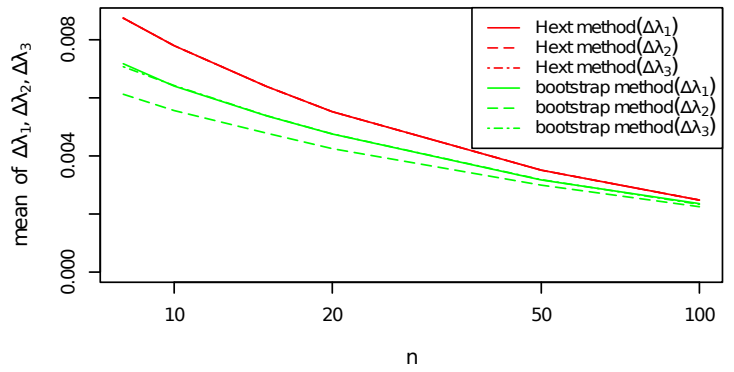
Figure 4

$U=0, P=1.01, \sigma=0.02$

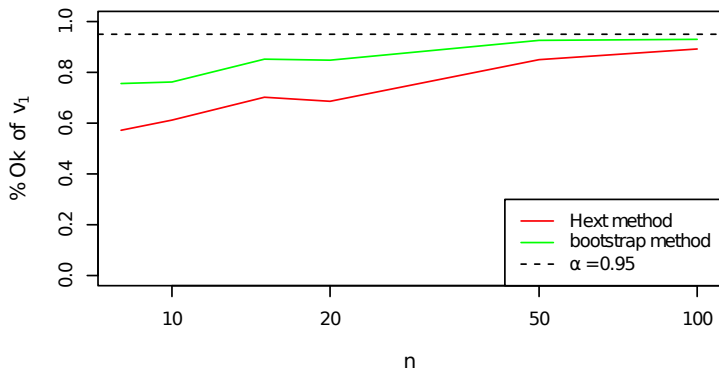
Success % for the eigenvalues



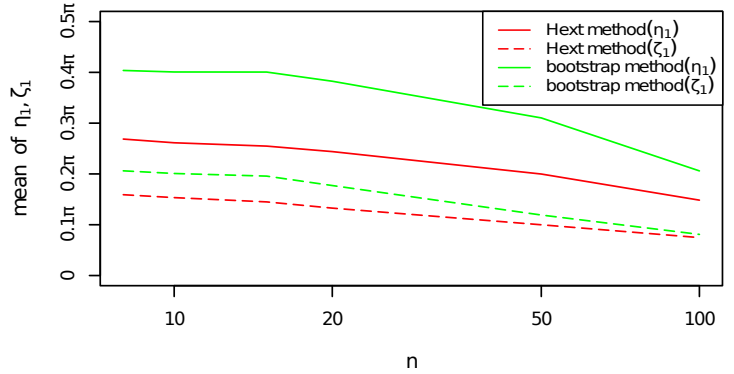
Mean errors for the eigenvalues



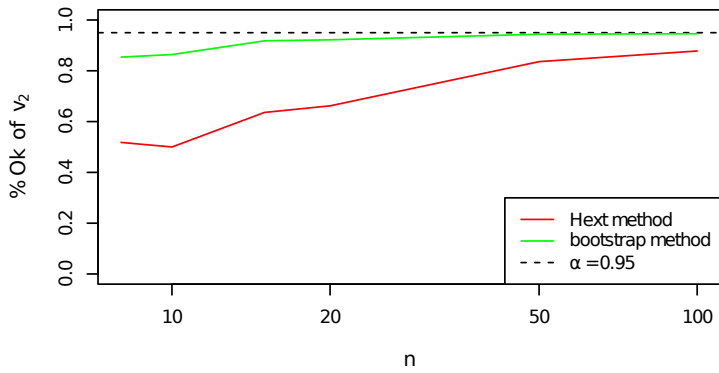
Success % for max eigenvector



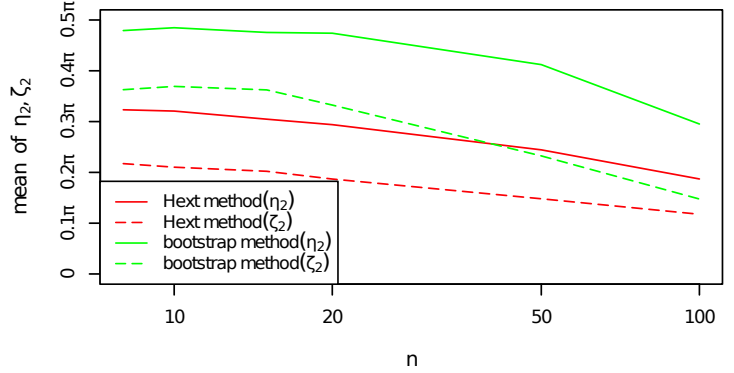
Mean errors for max eigenvector



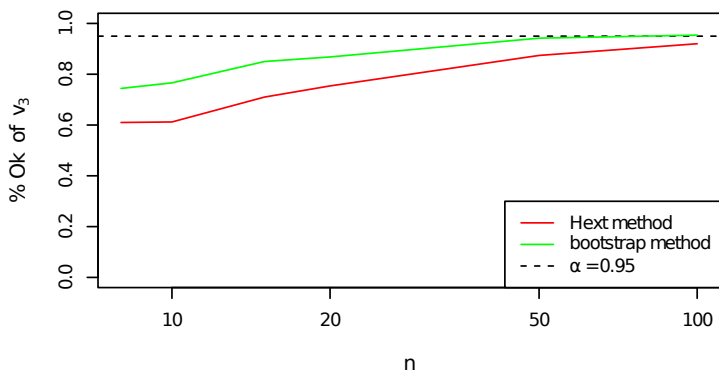
Success % for int eigenvector



Mean errors for int eigenvector



Success % for min eigenvector



Mean errors for min eigenvector

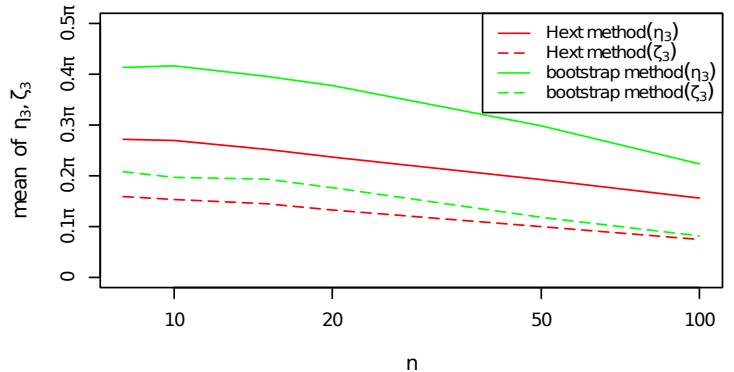
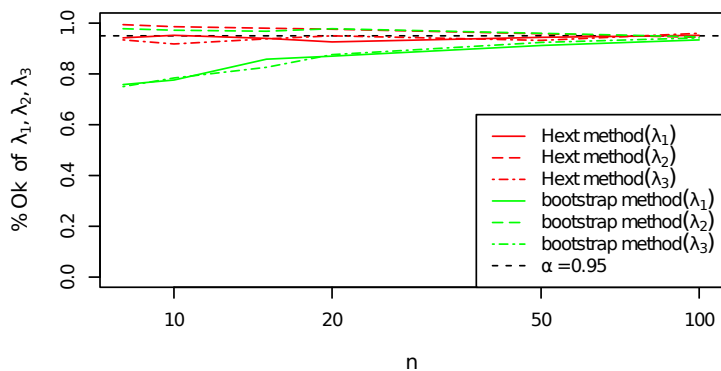


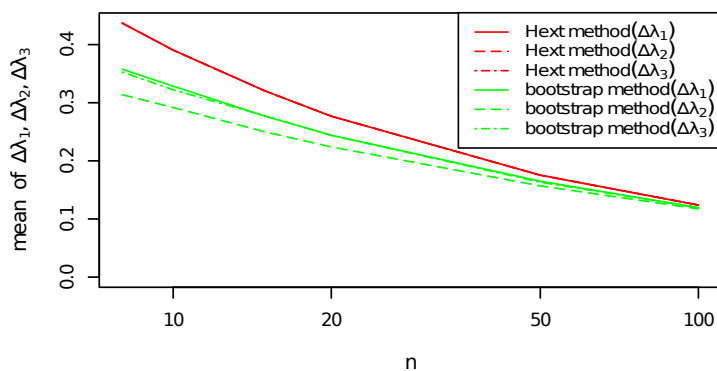
Figure 5

$U=0, P=2, \sigma=1$

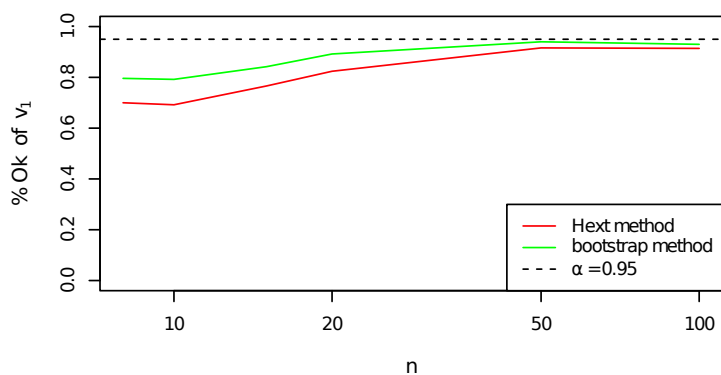
Success % for the eigenvalues



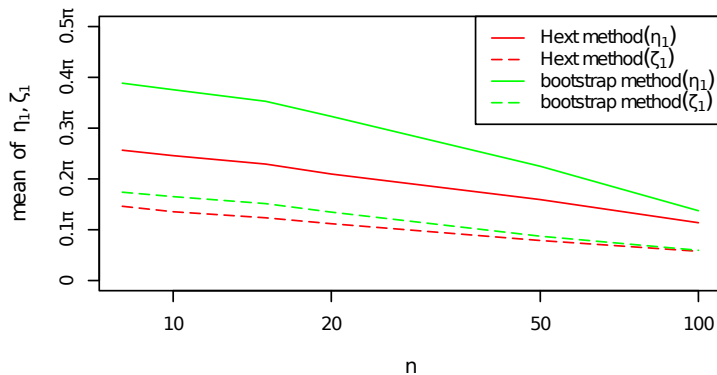
Mean errors for the eigenvalues



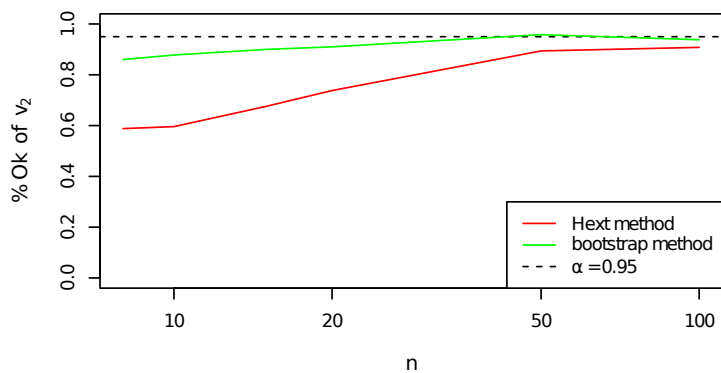
Success % for max eigenvector



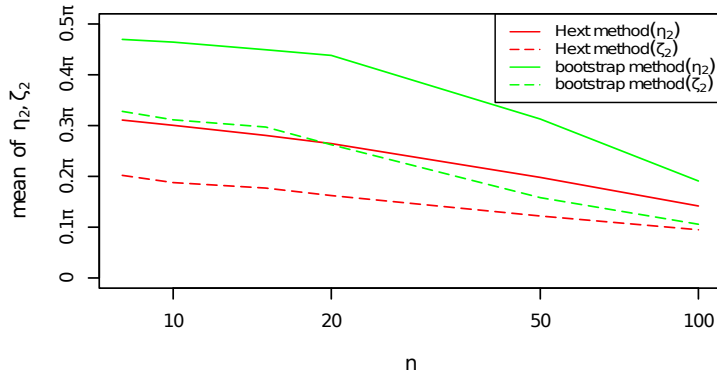
Mean errors for max eigenvector



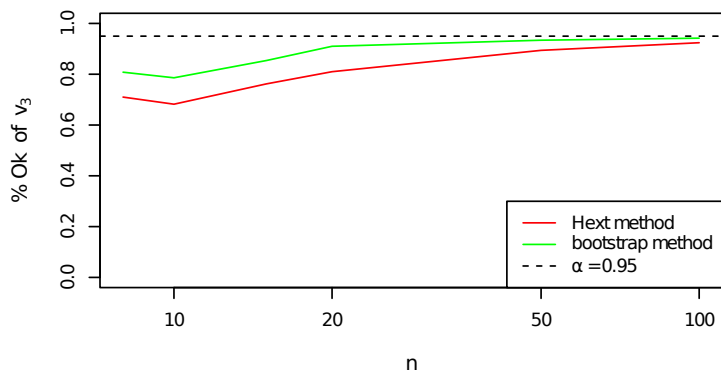
Success % for int eigenvector



Mean errors for int eigenvector



Success % for min eigenvector



Mean errors for min eigenvector

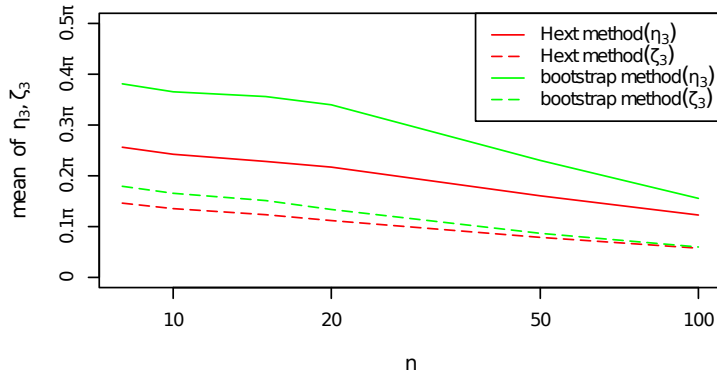
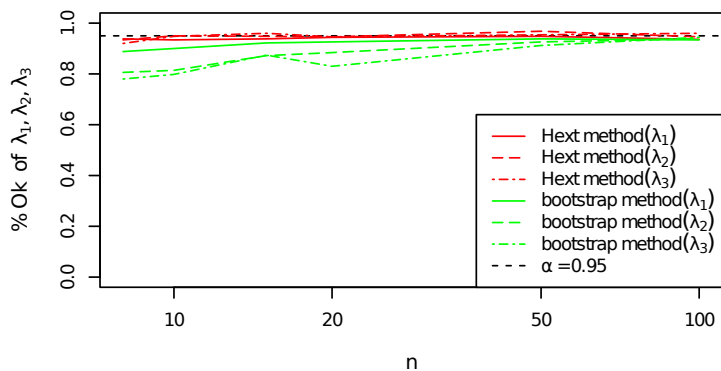


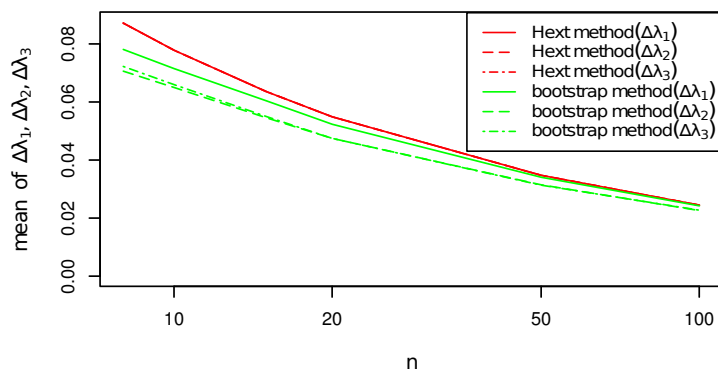
Figure 6

$U = -0.9, P = 2, \sigma = 0.2$

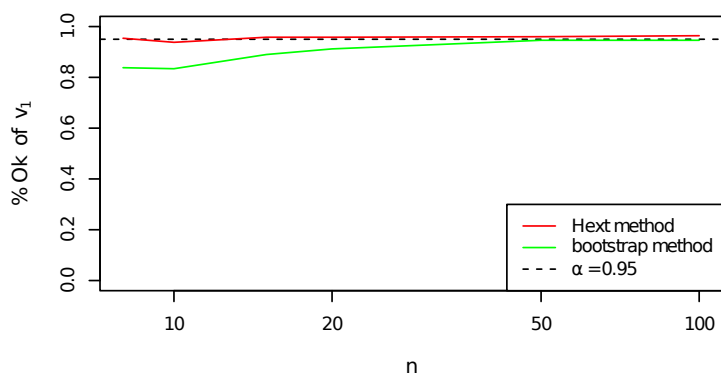
Success % for the eigenvalues



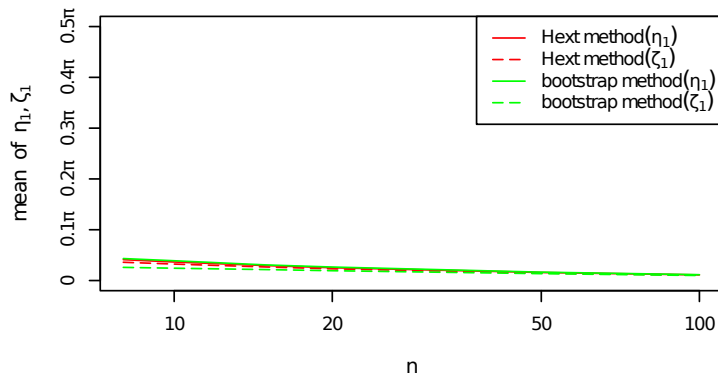
Mean errors for the eigenvalues



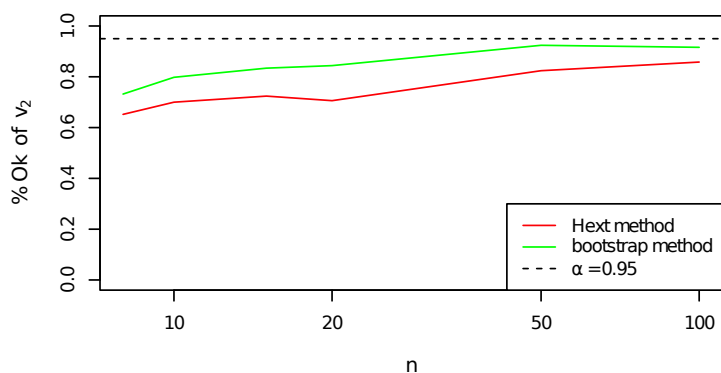
Success % for max eigenvector



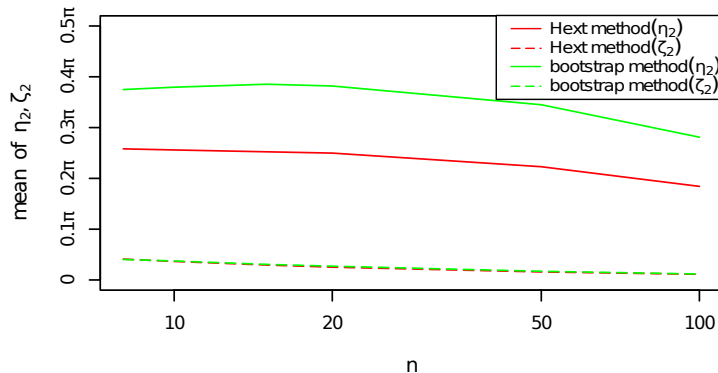
Mean errors for max eigenvector



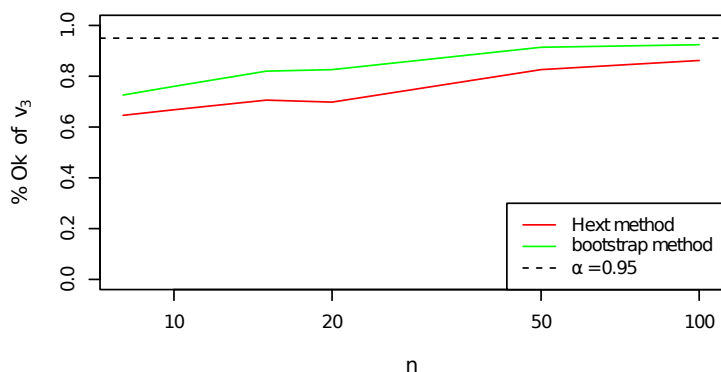
Success % for int eigenvector



Mean errors for int eigenvector



Success % for min eigenvector



Mean errors for min eigenvector

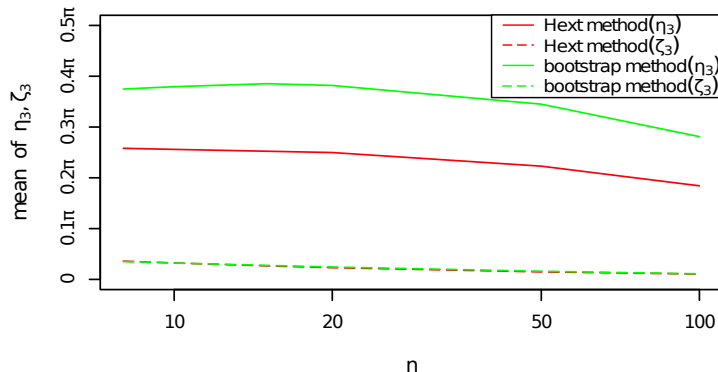
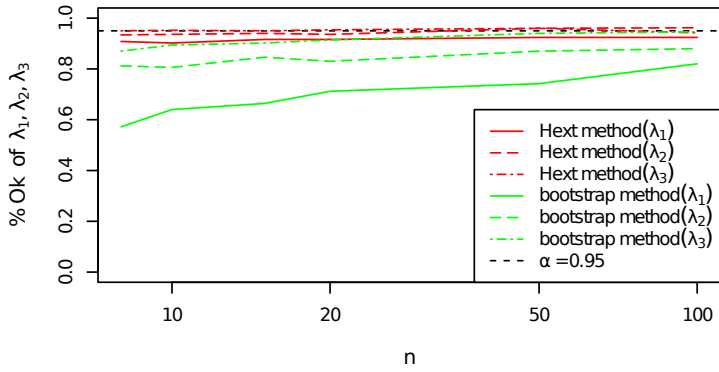


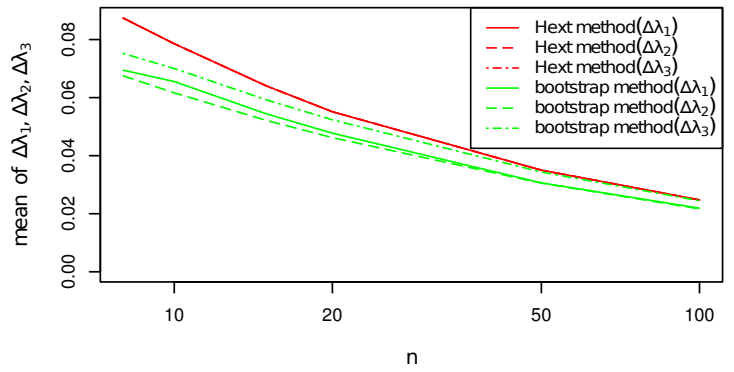
Figure 7

$U = 0.9, P = 1.01, \sigma = 0.01$

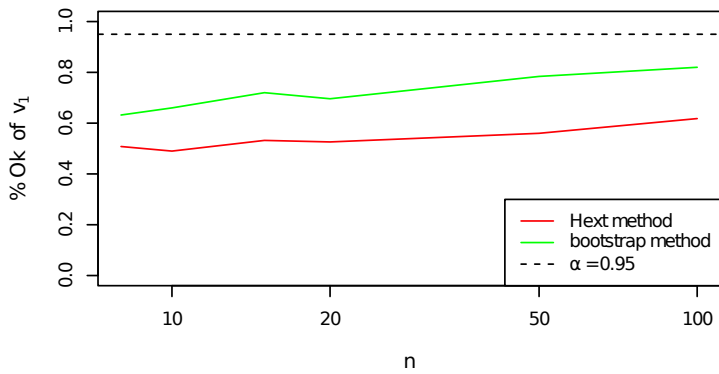
Success % for the eigenvalues



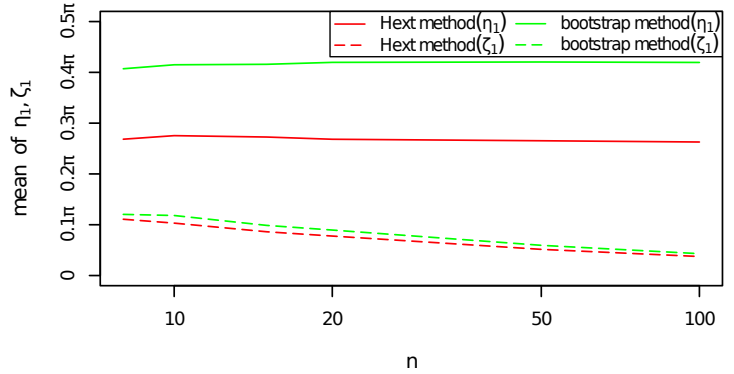
Mean errors for the eigenvalues



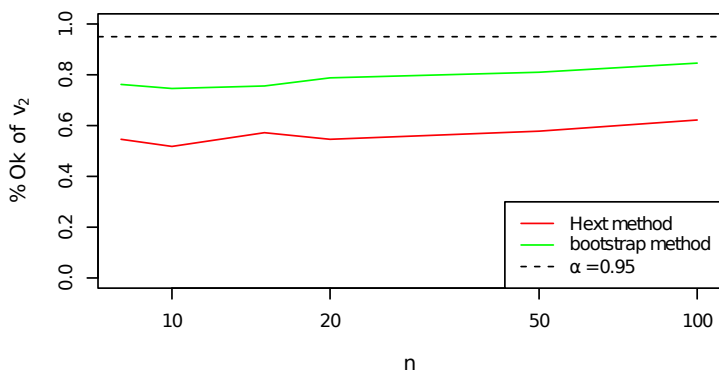
Success % for max eigenvector



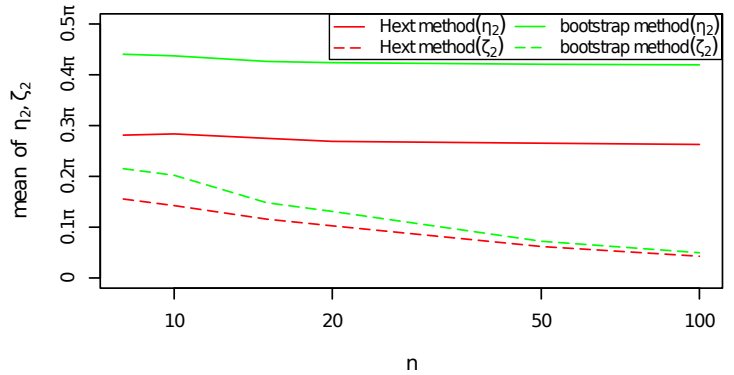
Mean errors for max eigenvector



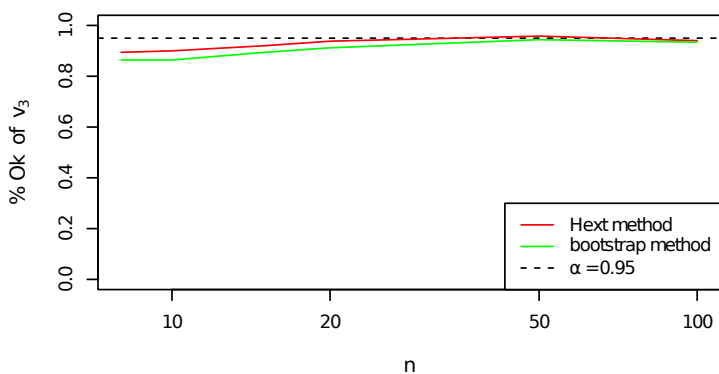
Success % for int eigenvector



Mean errors for int eigenvector



Success % for min eigenvector



Mean errors for min eigenvector

